Protein aggregation of the p63 transcription factor underlies severe skin fragility in AEC syndrome

Claudia Russo[a,1], Christian Osterburg[b,1], Anna Sirico[a,1], Dario Antonini[c,d], Raffaele Ambrosio[d], Julia Maren Würz[b], Jörg Rinnenthal[b,2], Marco Ferniani[c], Sebastian Kehrloesser[b,3], Birgit Schäfer[b], Peter Güntert[b], Satrajit Sinha[e], Volker Dötsch[b,4,5], and Caterina Missero[a,c,4,5]

[a]Centro di Ingegneria Gentica e Biotecnologie Avanzate, 80145 Naples, Italy; [b]Institute of Biophysical Chemistry and Center for Biomolecular Magnetic Resonance, Goethe University, 60438 Frankfurt, Germany; [c]Department of Biology, University of Naples Federico II, 80126 Naples, Italy; [d]Istituto di Ricovero e Cura a Carattere Scientifico (IRCCS) Istituto di Ricerca Diagnostica e Nucleare (SDN), 80143 Naples, Italy; and [e]Department of Biochemistry, Center of Excellence in Bioinformatics and Life Sciences, State University of New York, Buffalo, NY 14203

Edited by Carol Prives, Columbia University, New York, NY, and approved December 18, 2017 (received for review August 21, 2017)

The *p63* gene encodes a master regulator of epidermal commitment, development, and differentiation. Heterozygous mutations in the C-terminal domain of the *p63* gene can cause ankyloblepharon-ectodermal defects-cleft lip/palate (AEC) syndrome, a life-threatening disorder characterized by skin fragility and severe, long-lasting skin erosions. Despite deep knowledge of p63 functions, little is known about mechanisms underlying disease pathology and possible treatments. Here, we show that multiple AEC-associated p63 mutations, but not those causative of other diseases, lead to thermodynamic protein destabilization, misfolding, and aggregation, similar to the known p53 gain-of-function mutants found in cancer. AEC mutant proteins exhibit impaired DNA binding and transcriptional activity, leading to dominant negative effects due to coaggregation with wild-type p63 and p73. Importantly, p63 aggregation occurs also in a conditional knock-in mouse model for the disorder, in which the misfolded p63 mutant protein leads to severe epidermal defects. Variants of p63 that abolish aggregation of the mutant proteins are able to rescue p63's transcriptional function in reporter assays as well as in a human fibroblast-to-keratinocyte conversion assay. Our studies reveal that AEC syndrome is a protein aggregation disorder and opens avenues for therapeutic intervention.

AEC syndrome | mouse model | p63 | protein aggregation | skin

As a tetrameric transcription factor required for the development of stratified epithelia, p63 plays an essential role in the commitment of simple ectoderm to epidermal lineages and in the proliferative potential of epidermal stem cells (1–6). Its DNA binding domain (DBD) is highly homologous to the DBD of its family members, p53 and p73. Therefore, p63 binds to canonical p53 DNA-binding sites and shares some biological functions with the other members of the family (7, 8). The highly conserved oligomerization domain (OD) allows homotetramerization required for high DNA affinity (9), and hetero-tetramerization with p73 (10, 11). Due to the presence of two independent promoters, two classes of p63 proteins are expressed that differ at the amino (N)-terminus: TAp63 and ΔNp63. TAp63 protein is highly expressed in a dimeric inactive conformation in female germ cells during meiotic arrest (12, 13). DNA damage promotes the formation of active tetramers (9), leading to DNA damage-induced oocyte death (12). In contrast, the ΔNp63 proteins are found in a tetrameric form, and are primarily expressed in the basal regenerative layers of the epidermis and other stratified epithelia, where they play multiple essential roles in keratinocyte proliferation, differentiation, and cell adhesion (3, 5, 7, 14, 15). For most epidermal target genes, ΔNp63 acts as a transactivator, but it can also act as a repressor for other genes (3, 5, 16–19).

At least three distinct 3′ splice variants also exist: α, β, and γ. The α isoform is by far the most abundant isoform in stratified epithelia and contains a poorly characterized sterile-α-motif (SAM) domain, a putative protein interaction module present in a wide variety of proteins, and a post-SAM (PS) domain. The p63 SAM domain shows a typical five-helix bundle architecture (20, 21), is unable to form homodimers (21, 22), and its function remains unknown. The PS domain is about the same length as the SAM domain and can be divided in two subdomains. The N-terminal subdomain (45 amino acids) contains a transcriptional inhibitory (TI) sequence that forms a closed inactive dimer with the TA domain (23, 24). The C-terminal subdomain (25 amino acids) contains a sumoylation site involved in regulating p63's concentrations (24).

Heterozygous mutations in *p63* (*TP63*) are causative of a group of autosomal dominant human disorders characterized by various combinations of ectodermal dysplasia, orofacial clefting, and limb malformations (7, 25). Among these disorders, ectrodactyly, ectodermal dysplasia, and cleft lip/palate syndrome [EEC, Online Mendelian Inheritance in Man (OMIM) 604292] is mainly characterized by severe ectrodactyly and limb defects (26), whereas in ankyloblepharon-ectodermal defects-cleft lip/palate syndrome

Significance

The *p63* gene encodes a master regulator of epidermal development and function. Specific mutations in *p63* are causative of a life-threatening disorder mainly characterized by severe skin erosions and cleft palate. Little is known about the mechanisms underlying disease pathology and possible treatments. Based on biochemical studies, genetic mouse models, and functional assays, we demonstrate that these mutations cause p63 protein misfolding and aggregation. Protein aggregation lead to reduced DNA binding and impaired transcriptional activity. Importantly, genetic modifications of *p63* that abolish aggregation of the mutant proteins rescue its function, revealing that ankyloblepharon-ectodermal defects-cleft lip/palate syndrome is a protein aggregation disorder and opening avenues for therapeutic intervention.

Author contributions: V.D. and C.M. designed research; C.R., C.O., A.S., D.A., R.A., J.M.W., J.R., M.F., S.K., B.S., P.G., and S.S. performed research; C.R., C.O., A.S., D.A., V.D., and C.M. analyzed data; and C.R., C.O., A.S., D.A., V.D., and C.M. wrote the paper.

The authors declare no conflict of interest.

This article is a PNAS Direct Submission.

Data deposition: The NMR chemical shifts have been deposited in the Protein Data Bank, www.wwpdb.org (PDB ID code 5N2O).

[1]C.R., C.O., and A.S. contributed equally to this work.

[2]Present address: Boehringer Ingelheim RCV GmbH & Co KG, A-1121 Vienna, Austria.

[3]Present address: Cancer Research UK, Cambridge Institute, Li Ka Shing Centre, University of Cambridge, Cambridge CB2 0RE, United Kingdom.

[4]V.D. and C.M. contributed equally to this work.

[5]To whom correspondence may be addressed. Email: vdoetsch@em.uni-frankfurt.de or missero@ceinge.unina.it.

This article contains supporting information online at www.pnas.org/lookup/suppl/doi:10.1073/pnas.1713773115/-/DCSupplemental.

(AEC, OMIM 106260), the distinguishing features are ankyloblepharon, congenital erythroderma, skin fragility, atrophy, palmoplantar hyperkeratosis, and extensive skin erosions (21, 27). Distinct *p63* mutations can also cause nonsyndromic diseases, including isolated split hand/foot malformation (SHFM4, OMIM 605289) (28). For each of these diseases, mutations are generally clustered in specific p63 protein domains or are found in the same domain but have distinct characteristics, suggesting a genotype-to-phenotype correlation (25) (Fig. 1*A*). AEC syndrome mutations are predominantly clustered in the C-terminal portion of p63, either as missense mutations in the SAM domain and more rarely in the TI domain, or as single-base frameshift mutations that lead to elongation of the C-terminal domain (25).

It is generally believed that heterozygous *p63* mutations have a dominant-negative effect due to formation of mixed wild-type and mutant p63 tetramers, reducing the cellular amounts of functional p63. The fact that different mutations give rise to distinct phenotypes and syndromes, however, suggests distinct mechanisms of action of the mutants. Here, we report that the dominant-negative activity effects of AEC-associated *p63* mutations result from an increased aggregation propensity. Mutant p63 induces misfolding and coaggregation of wild-type p63, causing partial impairment in DNA binding and deficient transcription of target genes. This is observed both in heterologous cells expressing AEC mutant p63 proteins and in keratinocytes derived from a newly developed conditional knock-in mouse model for AEC syndrome. Mutant p63 also leads to coaggregation with its paralogue p73, possibly also leading to its inactivation. Relieving mutant p63 aggregation leads to reactivation of its function, indicating that aggregation is the cause of its impairment.

Results

Aggregation Is a Characteristic Feature of AEC Mutant p63 Proteins. AEC mutations cluster predominantly in the carboxyl (C) terminus of the p63α isoform and include several missense mutations in the SAM domain (e.g., L514F, G530V), two missense mutations in the TI domain (R598L, D601V), and several frameshift mutations leading to abnormal extensions of the C terminus (e.g., 3′ss intron 10, 1456InsA, 1709DelA, 1859DelA) (Fig. 1*A*). In contrast, the few EEC mutations found in the C terminus cause a premature stop codon (Fig. 1*A*), suggesting that missense mutations, extensions, or truncations of the C terminus differentially alter p63 function. The mechanisms by which AEC-causative mutations interfere with p63 functions has remained obscure, and we hypothesized that a selective structural alteration may be at the basis of this disorder. To test this hypothesis, we first determined the structure of L514F mutant SAM domain using NMR (Fig. 1*B* and *SI Appendix*, Fig. S1*A* and Table S1). L514 is a highly conserved amino acid in the first helix of the SAM domain, which is mutated to phenylalanine, serine, or valine in AEC patients (21, 29). The wild-type and L514F mutant structures revealed close similarity, with a backbone root mean square deviation (rmsd) value of 1.5 Å. The less compact fold of the mutant protein was caused by steric clashes due to the placement of the phenylalanine side chain in the hydrophobic core as previously predicted (30), likely leading to destabilization of the SAM domain.

To measure SAM domain destabilization, we monitored temperature-induced unfolding by circular dichroism (CD) spectroscopy (Fig. 1*C*). While the wild-type SAM domain showed a melting temperature of 79 °C, the mutant was destabilized with an unfolding temperature of 65 °C. In addition, only the unfolding of the wild-type SAM domain was reversible, while the L514F SAM domain mutant irreversibly precipitated upon unfolding (Fig. 1*D* and *SI Appendix*, Fig. S1*B*).

To investigate whether AEC mutants might be prone to destabilization and precipitation due to an increased aggregation propensity, we analyzed the p63 amino acid sequence using the TANGO algorithm that predicts aggregation prone regions (APRs) in proteins (31). This analysis indicated that two peptides (peptides 1 and 2), located in the first and third helix of the SAM domain, displayed some aggregation propensity, which was enhanced by the L514F and G530V mutations, respectively (Fig. 1*E*, *Lower* and *SI Appendix*, Fig. S1*C* and Table S2). Similarly, the two point mutations within the TI domain, R598L and D601V, strongly enhanced the low intrinsic aggregation propensity of the TI domain (Fig. 1*E*, *Lower* and *SI Appendix*, Table S2). Finally, TANGO analysis was performed for 3′ss-int10 and 1456InsA, and on the 1709DelA and 1859DelA mutants that lead to frameshifts and two different extensions of the C terminus, respectively. Aberrant elongations of the mutant proteins generated APRs (peptides I, II, III) (Fig. 1*E* and *SI Appendix*, Fig. S1*D* and Table S2). In contrast, EEC-associated frameshift mutations in the C terminus 1572InsA, 1576DelTT, and 1743DelAA did not create new peptides predicted to lead to aggregation (*SI Appendix*, Table S2), suggesting that the generation, exposure, or enhancement of APRs is a characteristic feature of AEC syndrome.

To assess whether AEC-associated mutant p63 proteins have the propensity to form aggregates in mammalian cells, wild-type and mutant p63 were overexpressed in H1299 cells that are devoid of p53 and its family members, and run on Blue-Native polyacrylamide gel electrophoresis (BN-PAGE) followed by Western blotting. Transiently overexpressed wild-type p63 and EEC mutations (R304Q, 1576DelTT, 1743DelAA, 1572InsA) run primarily as monomers (Fig. 1*F*), in agreement with the short half-life of the p63 tetramer compared with that of other p53 family members (32). In contrast, overexpression of p63L514F and all other tested AEC mutants caused a shift in molecular mass, consistent with the formation of large multimeric assemblies (Fig. 1*F*). Such aggregation was similar to that observed for the conformation mutant of p53 (R175H), known to be destabilized and to aggregate (33), whereas the p53 DNA contact mutant R248W did not aggregate (*SI Appendix*, Fig. S1*E*). Similar results were obtained by size exclusion chromatography (SEC), in which most of the p63L514F mutant protein eluted at high molecular weight (Fig. 1*G*) similarly to p53R175H mutant protein (*SI Appendix*, Fig. S1*G*), whereas wild-type p63 eluted at low molecular weight.

AEC Mutant p63 Selectively Binds to p53 Family Members. The oncogenic gain-of-function activities attributed to mutant p53 have been correlated to aberrant binding and coaggregation with wild-type p63 and p73 (33). We previously reported that binding of p53 mutants to p63 is dependent on the low but detectable aggregation tendency of the p63 TI domain (Fig. 1*E* and *SI Appendix*, Table S2) (32). Such aggregation tendency is completely abolished by the p63V603D mutant that is unable to bind p53 (32). To test whether the aggregation propensity of AEC mutants in the SAM domain is dependent on the mild intrinsic aggregation propensity of the TI domain, we tested AEC mutants in the background of the V603D mutation. All AEC mutants in the SAM domain exhibited severe aggregation even in the V603D background, while the wild-type and EEC mutants (R279H, R304Q) displayed no residual aggregation as shown by BN-PAGE and SEC (Fig. 2 *A* and *B*). Accordingly, AEC-associated mutants strongly bound to mutant p53 even in the V603D background, whereas no binding was observed for EEC mutants (Fig. 2*C*). Aggregation of AEC mutants was temperature-dependent, as p63L514F/V603D aggregation progressively increased at physiological temperature, whereas no aggregation was observed in either p63V603D or p63R304Q/V603D even at high temperature (*SI Appendix*, Fig. S2*A*). Taken together, these data indicate that AEC mutants have a strong tendency of aggregating, and that AEC mutations in the SAM domain cause aggregation independently of the TI domain.

To investigate whether AEC-associated mutant p63 may coaggregate with wild-type p63, we cotransfected HA-tagged wild-type p63 with Myc-tagged wild-type or AEC mutant p63. Interestingly, even in the V603D background, the SAM domain mutant

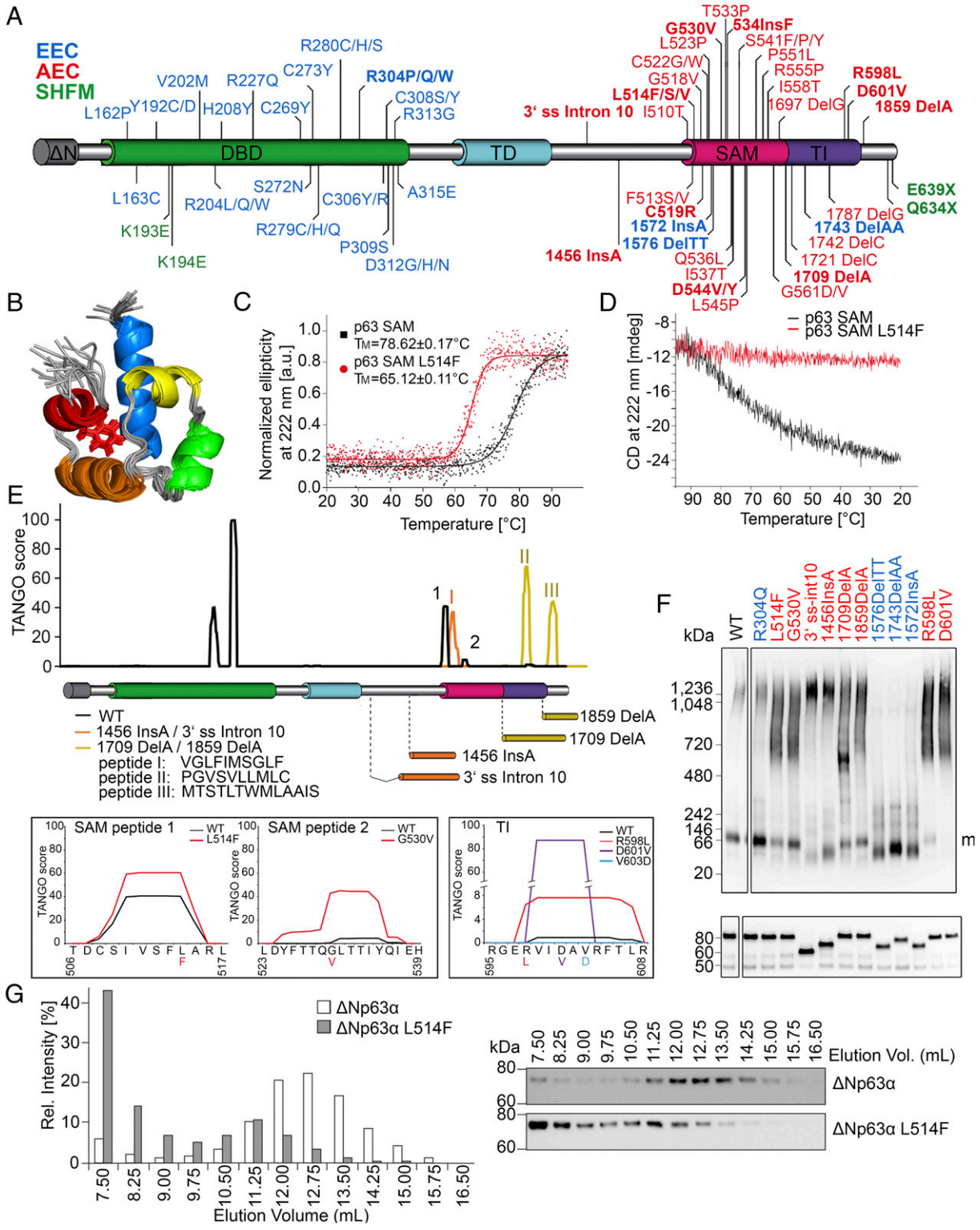

Fig. 1. Aggregation propensity of AEC mutant p63. (*A*) p63 structure and disease-causative mutations (color-coded for each disease as indicated). In bold are mutations used in this study. (*B*) NMR spectroscopy of the murine L514F SAM (PDB ID code 5N2O). Bundle of 20 conformers with the lowest CYANA target function values is shown. The mutated amino acid is indicated as a stick. (*C*) Melting curves of the purified wild-type (black) and L514F (red) SAM domain were recorded by CD spectroscopy. (*D*) Reverse CD melting curves of the purified wild-type and L514F SAM domain after recording the initial melting curve. The mutant remained unfolded due to irreversible precipitation. (*E*) TANGO analysis for the wild-type ΔNp63α (in black) and for the indicated AEC mutations caused by protein elongation (*Upper*: aggregating peptide I-III) or missense mutations in the SAM and TI domains (*Lower*). The V603D variant is predicted to abolish mutant aggregation. (*F*) BN-PAGE (*Upper*) and SDS/PAGE (*Lower*) followed by Western blot for p63 in H1299 extracts expressing wild-type (WT) and the EEC (blue) or the AEC (red) mutations. Soluble ΔNp63α protein runs mainly as a monomer (m). (*G*) SEC followed by Western blot of H1299 cell lysates overexpressing wild-type ΔNp63α and p63L514F mutant. Samples were incubated at 37 °C for 15 min before loading on SEC. Bar diagrams on the *Left* show the relative intensities of each collected fraction.

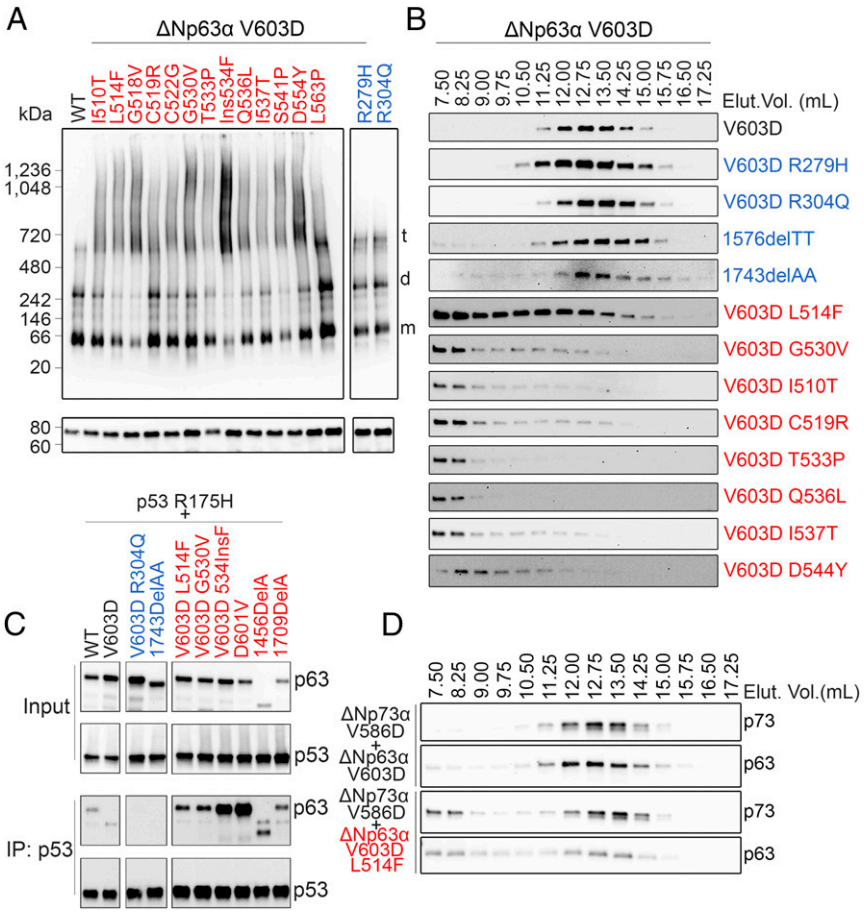

Fig. 2. AEC-associated p63 mutants aggregate with other p53 family members. (*A*) BN-PAGE (*Upper*) and SDS/PAGE (*Lower*) followed by Western blot of the wild-type p63 and an extended set of AEC mutations in the SAM domain in the ΔNp63αV603D variant background (*Left*) and EEC mutant (*Right*) transiently expressed in H1299 cells. (*B*) SEC analysis and Western blot of wild-type and the indicated mutant p63 expressed in H1299 cells. Wild-type ΔNp63α and all EEC mutant proteins elute as tetramers (11.25–15 mL), while AEC mutants are mainly shifted to the void volume (7.5 mL), corresponding to aggregates. (*C*) Coimmunoprecipitation between mutant HA-p53R175H and the indicated Myc-ΔNp63α proteins. p53 was immunoprecipitated (IP) with an HA-specific antibody. Anti-HA Tag antibodies were used to detect p53, whereas anti-Myc antibodies were used for p63. (*D*) SEC analysis and Western blot of ΔNp73α V586D (corresponding to V603D in p63) coexpressed with ΔNp63α V603D either wild-type or L514F in H1299 cells. Samples were incubated at 37 °C for 15 min before loading on SEC.

aggregated with wild-type p63 (*SI Appendix*, Fig. S2*B*), indicating that it may exert a dominant negative function.

As previously shown for wild-type p63 (10, 11), AEC mutant p63 bound p73 (*SI Appendix*, Fig. S2*C*). A p73 mutant protein with no propensity to self-aggregate (p73V586D) (32) aggregated in the presence of mutant p63L514F/V603D, but not with p63V603D alone (Fig. 2*D*). In contrast neither wild-type nor AEC mutant p63 interacted with wild-type p53 (*SI Appendix*, Fig. S2*D*), and no increase in p53 aggregation was observed in the presence of AEC mutant p63 (*SI Appendix*, Fig. S2*E*). Taken together, these data indicate that AEC-associated p63 mutants cause aggregation not only of their wild-type p63 counterpart, but also of wild-type p73, revealing that AEC-associated p63 mutants may display gain-of-function activities through coaggregation with selected family members.

Protein Aggregation Is Associated with Impaired Transcriptional Function in a Mouse Model for AEC Syndrome. To investigate the effect of AEC-associated mutations on ΔNp63α function, we tested the ability of a variety of mutants (Fig. 1*A*) to transactivate the regulatory regions of two crucial p63 target genes, namely keratin 14 (KRT14) and fibroblast growth factor receptor 2 (FGFR2) (15, 34, 35). As previously reported (15, 36), wild-type ΔNp63α efficiently activated the KRT14 promoter as well as the FGFR2 enhancer in HEK293 cells, whereas an EEC causative mutation that directly impairs DNA binding (R304Q) abolished p63 activity (*SI Appendix*, Fig. S3*A*). All tested AEC-associated mutations, including missense mutations in the SAM and TI domains and frameshift mutations, invariably abolished or severely reduced p63 transcriptional activity, whereas two missense mutations in the PS domain causative of SHFM syndrome (Q630X and E635X) retained transactivation activity in this context.

To test whether impaired transcriptional activity of AEC-associated p63 mutants affected its biological function in a more physiological context, we took advantage of a recently developed protocol to convert human dermal fibroblasts (HDFs) into induced keratinocyte-like cells (iKCs) by coexpression of ΔNp63α and Krüppel-like factor 4 (KLF4) (37). Eighteen days after p63/KLF4 transduction, HDFs had converted into iKCs and expressed keratinocyte-specific p63 transcriptional targets, including KRT14 (5, 35), the IFN regulatory factor 6 (IRF6) involved in keratinocyte differentiation (38–40), and desmocollin 3 (DSC3) encoding a desmosome component expressed in basal keratinocytes (14) (Fig. 3 *A* and *B*). In contrast, similarly to the EEC mutant R304Q, AEC mutants were unable to induce expression of keratinocyte-specific target genes, indicating that they are functionally incapable to convert HDFs into iKCs.

To assess whether loss of p63 activity occurs in vivo, we generated a mouse model for AEC syndrome. We have previously shown that a constitutive p63 L514F knock-in mouse phenocopies the clinical

hallmarks of the human disorder at least in part through impaired FGFR2 signaling required for the expansion of epidermal progenitor cells during embryonic development (15, 41). However, the constitutive p63 L514F knock-in mouse line could not be maintained due to fully penetrant cleft palate and consequent perinatal lethality (15). Therefore, we used a conditional knock-in strategy to create L514F mutant mice ($p63^{L514Fflox/L514Fflox}$) in which the AEC-associated mutation L514F is only expressed in the presence of Cre recombinase (Fig. 3 *C* and *D*, and *SI Appendix*, Fig. S3 *B–D*). We first tested the expression of p63 target genes in primary keratinocytes isolated from p63L514F mice infected with an adenovirus carrying the Cre recombinase (Ad-Cre) or a mock control. Target genes previously reported to be positively regulated by p63 and affected in AEC syndrome (14, 15, 35, 40, 42) were strongly reduced in Ad-Cre–infected homozygous keratinocytes and to a lesser extent in heterozygous keratinocytes compared with Ad-GFP controls (Fig. 3 *E* and *F*), confirming that endogenous mutant p63L514F has an impaired transactivation ability. Interestingly, expression of genes repressed by p63, such as Smad7 and Krt8 (5, 17) were derepressed in the presence of the L514F mutant compared with controls (Fig. 3*G*), demonstrating that both transactivation and repression functions of p63 are impaired by AEC mutations.

$p63^{L514Fflox/L514Fflox}$ mice were crossed with K14-Cre knock-in mice carrying the Cre recombinase under the control of the endogenous Krt14 promoter that is active in stratified epithelia from embryonic day 17.5 (43), leading to uniform p63 mutant expression from P0 (Fig. 3*H*). K14-Cre; $p63^{L514Fflox/L514Fflox}$ homozygous mice displayed ectodermal defects and skin erosion typical of AEC syndrome (Fig. 3*I*). Primary keratinocytes isolated from K14-Cre; $p63^{L514Fflox/L514Fflox}$ mice exhibited strongly decreased levels of crucial p63 target genes (Fig. 3*J*).

To test whether mutant p63L514F protein exhibited propensity toward aggregation endogenously, we performed BN-PAGE followed by Western blotting on keratinocyte lysates. As expected, p63 from wild-type keratinocytes mainly runs as a monomer. In contrast, the monomeric form was reduced and large multimeric assemblies were observed in Ad-Cre–infected $p63^{+/L514Fflox}$ keratinocyte lysates, whereas in Ad-Cre–infected $p63^{L514Fflox/L514Fflox}$ keratinocyte lysates, the monomeric form was lost (Fig. 3*K*). Similar results were observed with primary keratinocytes derived from Krt14-Cre;$p63^{+/L514Fflox}$ and Krt14-Cre;$p63^{L514Fflox/L514Fflox}$ mice compared with $p63^{L514Fflox/L514Fflox}$ controls (Fig. 3*L*).

Taken together these data indicate that AEC-associated p63 mutations impair the ability of p63 to act both as a transcriptional activator and as a repressor in vivo, and that the impairment is associated with progressive p63 aggregation in the presence of the mutant form.

Aggregation of AEC-Associated p63 Mutants Causes Impaired DNA Binding. To test whether aggregation of AEC mutants alters the ability of p63 to bind DNA, chromatin immunoprecipitation followed by quantitative PCR (ChIP-qPCR) was performed in HEK293 cells transfected with wild-type and/or mutant p63. As previously reported, the EEC-associated mutant R304Q did not bind to well-characterized p63 genomic binding sites in *KRT14*, and *p63* genes that are positively regulated by p63, or to a p63 binding site in the *CDKN1A* promoter negatively regulated by p63 (3, 5, 15, 44, 45) (Fig. 4*A* and *SI Appendix*, Fig. S4 *A–E*). Surprisingly, even though the AEC mutations do not fall in the DNA binding domain, reduced DNA binding was observed for all AEC-associated mutants, whereas the SHFM-associated mutants efficiently bound DNA. DNA binding was also impaired when wild-type p63 was cotransfected with the L514F mutant, indicating that the mutant exerts a dominant negative effect on p63 DNA binding (Fig. 4*B*). Similarly reduced DNA binding was observed by electrophoretic mobility shift assay (EMSA) in HEK293 nuclear extracts (*SI Appendix*, Fig. S4F).

To assess the physiological relevance of these findings, the ability of p63 to bind DNA was tested in mouse primary keratinocytes within previously characterized p63 binding sites for positively regulated genes (*Irf6*, *Fgfr2*, and *Trp63*) (15, 40, 44) or for a negatively regulated gene *Smad7* (17). A significant reduction in p63 binding to DNA was detected in $p63^{L514Fflox/L514Fflox}$ knock-in keratinocytes, infected with Ad-Cre compared with controls for all tested binding sites (Fig. 4 *C* and *D*). Taken together these data indicate that the ability of p63 to bind DNA is weakened by mutations in the p63 C terminus causative of AEC syndrome.

To evaluate if reduced DNA binding is due to aggregation, we performed DNA pulldown experiments of in vitro translated proteins under conditions in which all mutant and wild-type proteins had a tetrameric conformation and did not form aggregates as assessed by SEC (*SI Appendix*, Fig. S4*G*). While EEC mutants R204W and R304Q had an intrinsic DNA binding impairment, AEC mutants L514F and G530V efficiently bound to DNA at similar levels as the wild-type protein (Fig. 4*E*).

Taken together, these results indicate that the DNA binding ability of AEC mutants is not intrinsically impaired, but rather is weakened, likely due to structural alterations and consequent protein aggregation that occurs in cells.

Transcriptional Activity Is Restored by Reducing the Aggregation Propensity of AEC-Associated Mutant p63. We next investigated whether reversing aggregation would be sufficient to restore transcriptional activity of AEC mutants. To this end we introduced point mutations predicted by TANGO to alleviate aggregation, or we deleted APRs. For the p63L514F mutant, aspartic acids were introduced in each of the two APRs in the SAM domain of the p63L514F mutant (Fig. 1*E*, SAM peptide 1 and 2, *SI Appendix*, Fig. S5*A* and Table S3). Aggregation was alleviated to various extents upon introducing single mutations in either peptide (V511D or F513D for peptide 1, and T533D or I534D for peptide 2), or combinations V511D/I534D, F513D/T533D, and F513D/I534D. Importantly, the double V511D/T533D substitution completely abolished aggregation of the L514F mutant (Fig. 5*A*). Next, we deleted APRs generated by frameshift mutations (Fig. 1*E* and *SI Appendix*, Fig. S1*D*). Deletion of peptide I for the splice mutant 3′ ss-int10, peptide II and III for the 1709DelA, and peptide III for the 1859DelAV603D frameshift mutants completely inhibited their aggregation (Fig. 5*B* and *SI Appendix*, Fig. S5*B*). Finally, we tested the possibility that the V603D mutation could abolish the aggregation propensity of the adjacent mutations R598L or D601V in the TI domain as predicted by TANGO (*SI Appendix*, Fig. S5*A* and Table S2). Introduction of the V603D mutation indeed inhibited aggregation of the R598L or D601V completely or to a large extent, respectively (Fig. 5*C*).

We next used transactivation assays to test whether abolishing aggregation rescued the transcriptional activity of p63 mutants. Consistent with the aggregation data, L514F and L514F/V603D mutants were inactive in luciferase assays, whereas L514F/V603D bearing the V511D/T533D double mutation exhibited restored transcriptional activity (Fig. 5*D*). Similarly, p63 transcriptional activity was fully restored upon deletion of the APRs in the elongated C-terminal domain caused by the frameshift mutations 1709DelA and 1859DelA (Fig. 5*E*). Finally, the V603D variant completely rescued the activity of the two point mutants R598L and D601V in the TI domain (Fig. 5*G*).

The weakened ability of the aggregation mutants to execute transcriptional modulation might explain the disease phenotype observed in AEC patients. To directly test the functional consequence of the increased aggregation for keratinocyte homeostasis, we resorted to the HDF to iKC conversation assay that is otherwise impaired by AEC mutations (Fig. 3 *A* and *B*). Deleting the aggregation peptides of the 1709DelA mutant or introducing V603D into the R598L mutant fully rescued their ability to induce expression of KRT14 and IRF6 in HDF (Fig. 5 *G* and *H*). Similarly, alleviating aggregation of the p63L514F mutant rescued its ability to convert HDF to iKC (Fig. 5*H*).

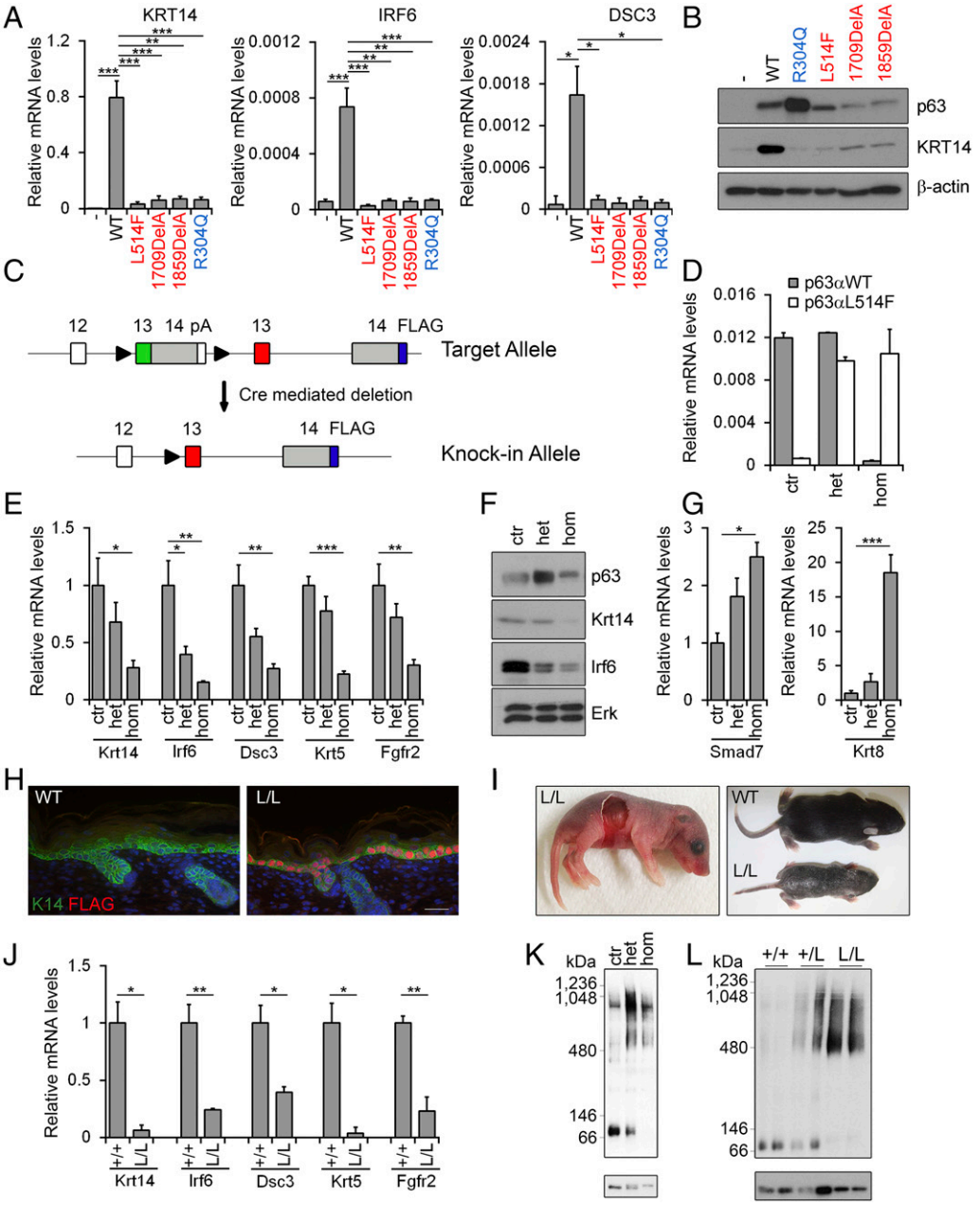

Fig. 3. p63 aggregation and impaired transcriptional function in a mouse model of AEC syndrome. (*A*) Real-time RT-PCR of the indicated keratinocyte-specific p63 target genes in HDFs converted to iKCs by coinfection with Klf4 and the indicated p63 viruses. (*B*) Western blot of Krt14 and p63 in iKCs. β-actin was used as loading control. (*C*) Gene targeting strategy for the $p63^{+/L514Fflox}$ knock-in mice. Mutant exon 13 carrying the L514F mutation is indicated in red. LoxP sites (black triangles) flank wild-type exon 13 (green) fused with the coding portion of exon 14 and the SV40 polyA (pA). 3xFLAG (blue) was placed at the end of the coding sequence in exon 14. FLAG-tagged p63 mutant protein is expressed upon Cre mediated deletion. (*D*) Real-time RT-PCR of wild-type p63 (gray bars) and p63L514F (white bars) in keratinocytes derived from $p63^{+/floxL514F}$ (het) and $p63^{L514Fflox/L514Fflox}$ (hom) mice after Ad-Cre–mediated deletion or after infection with Ad-GFP (ctr). (*E*) Real-time RT-PCR of target genes induced by p63 in mutant keratinocytes with ctr levels set to 1 ($n = 5$). (*F*) Western blot for p63 and the protein products of its target genes Krt14 and Irf6 in mutant keratinocytes. ERK was used as loading control. (*G*) Real-time RT-PCR of p63 repressed target genes in mutant keratinocytes ($n = 3$). (*H*) Immunofluorescence for K14 (green) and FLAG-tagged p63L514F (red) in epidermis of wild-type (WT) and K14-Cre; $p63^{L514Fflox/L514Fflox}$ (L/L) mice at P0. (Scale bars: 50 μm.) (*I*) Macroscopic phenotype of L/L mutant mice. Approximately 10% of newborn mice displayed large areas of skin erosions (*Left*). Skin crusting and ulcerations with reduced body size and dehydration were observed at P7-P8 in 100% of mutant mice (*Right*). (*J*) Real-time RT-PCR of p63 target genes in +/+ and L/L epidermis ($n = 6$). (*K*) BN-PAGE (*Upper*) and SDS/PAGE (*Lower*) followed by Western blot for p63 in mouse primary keratinocytes infected with Ad-Cre or Ad-GFP as in *D*. (*L*) BN-PAGE (*Upper*) and SDS/PAGE (*Lower*) followed by Western blot for p63 in primary keratinocytes isolated from mice with the indicated genotypes. Data are shown as mean ± SEM with the exception of *D* in which error bars indicate SD. Statistical significance was assessed using paired two-tailed *t* test (*J*) and one-way ANOVA analysis (*A*, *E*, and *G*). $*P \leq 0.05$; $**P \leq 0.001$; $***P \leq 0.0001$.

Finally, when exogenously expressed in wild-type keratinocytes, deleterious mutants p63L514F and p63R598L led to partial p63 aggregation and induction of Krt8 expression, a marker of simple epithelial tissues repressed by wild-type p63 and aberrantly expressed in knock-in mutant keratinocytes (Fig. 3*G*) (5). Importantly, p63 aggregation and Krt8 expression were suppressed by expression of rescue mutants (p63L514FV603D/V511D/T533D and R598LV603D) (*SI Appendix*, Fig. S5 *C* and *D*).

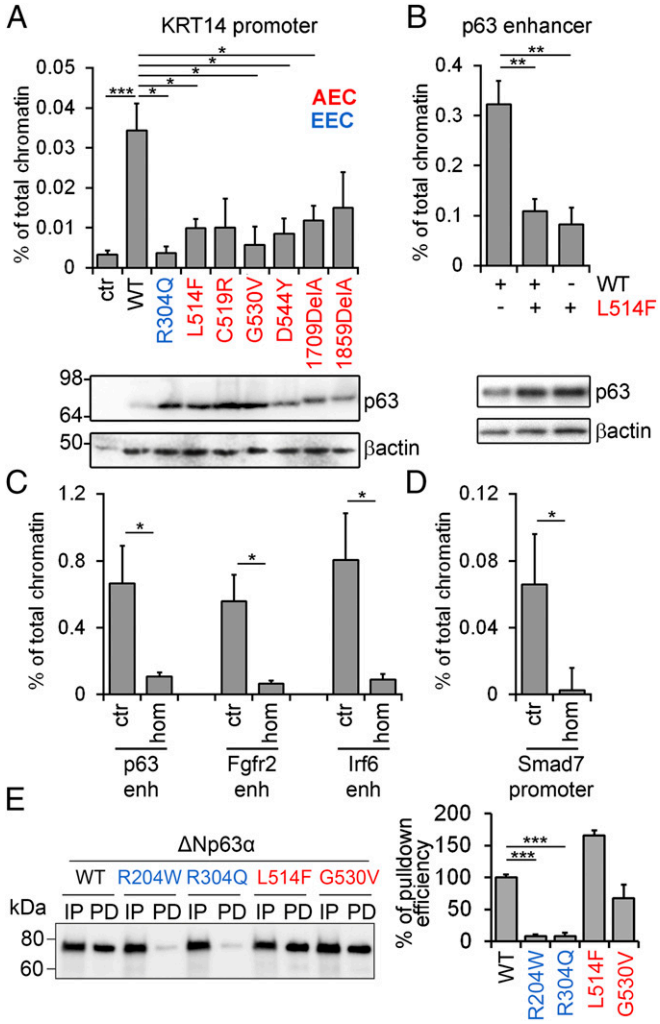

Fig. 4. AEC-associated p63 mutant proteins exhibit impaired DNA binding in cells. (*A*) ChIP-qPCR of the KRT14 promoter from HEK293 cells overexpressing p63 wild-type (WT) and the indicated mutants ($n = 6$) (*Upper*) and SDS/PAGE (*Lower*) followed by Western blot for p63 and β-actin (*Lower*). (*B*) ChIP-qPCR of the p63 enhancer from HEK293 cells cotransfected with p63 WT and p63L514F ($n = 5$) and relative SDS/PAGE (*Lower*) as in *A*. (*C*) ChIP-qPCR of the indicated p63-responsive enhancers in primary keratinocytes derived from $p63^{L514Fflox/L514Fflox}$ (hom) mice infected with Ad-Cre. Keratinocytes infected with Ad-GFP were used as controls (ctr) ($n = 4$). (*D*) ChIP-qPCR of the indicated p63-repressed gene element in primary keratinocytes under conditions as in *C* ($n = 3$). (*E*) Pulldown (PD) assay and Western blot of in vitro translated p63 with immobilized DNA oligonucleotides corresponding to the p63 responsive element on the human CDKN1A promoter. Input (IP). Percentage of pulldown efficiency is shown in the *Right* ($n = 3$). Data are shown as mean ± SEM with the exception of *E* in which error bars indicate SD. Statistical significance was assessed using paired two-tailed *t* test (*C* and *D*) and one-way ANOVA (*A*, *B*, and *E*). $*P \leq 0.05$; $**P \leq 0.001$; $***P \leq 0.0001$.

Taken together, these data indicate that missense mutations in the SAM domain or TI domain, or frameshift mutations leading to AEC syndrome, cause p63 protein aggregation and loss of transcriptional activity. Alleviating aggregation by mutating or removing amino acids responsible for the aggregation is sufficient to restore p63 transcriptional function.

Discussion

Among the p63-associated disorders, AEC syndrome is uniquely characterized by long-lasting and life-threatening skin erosions. Despite the severity of the symptoms, molecular studies have been hampered by the paucity of human biological material, and the poor understanding of the molecular mechanisms underlying the disorder. Here, we have shown that *p63* mutations associated with AEC syndrome cause reduced DNA binding and transcriptional activity due to mutant protein aggregation. Aggregation is caused by either aberrant protein elongation introducing aggregation-prone peptides, enhancing the intrinsic low APR of the TI domain, or by conformational changes that expose peptides with a natural high aggregation propensity. The latter is equivalent to the well-known gain-of-function mutations of p53 in cancer (e.g., R175H). AEC-associated p63 mutant proteins coaggregate with their wild-type counterpart and with p73. Importantly, the aggregation can be reversed and transcriptional activity of p63 rescued upon the introduction of specific point mutations that disrupt aggregation-prone peptides or upon their deletion.

To determine the relevance of these findings in vivo, we utilized a newly developed mouse model for AEC syndrome. We showed that endogenous mutant p63 in AEC mouse keratinocytes exhibits aberrant aggregation and inactivation of both transcriptional activating and repressing functions. This suggests that AEC mutations are unlikely to selectively impair interactions between p63 and specific coactivators or corepressors, but rather cause protein conformational changes that alter p63 function. The partial impairment in DNA binding observed for AEC mutants indicates that the propensity to form aggregates affects p63 affinity for DNA. This impairment, however, is not an intrinsic property of the AEC mutants but rather an indirect consequence of aggregation. DNA binding impairment therefore depends on the degree of aggregation and the effective removal of aggregates. This might partially explain differences in severity of the symptoms observed in different patients bearing the same mutation (25, 46), and differences in severity between patients diagnosed with AEC syndrome and Rapp–Hodgkin syndrome (OMIM 129400), diseases that have been suggested to be variable manifestations of the same clinical entity caused by overlapping p63 mutations in the carboxyl terminal domain (47, 48).

Aggregating proteins can inactivate other proteins through coaggregation. Three categories of proteins affected by mutant p63 can be distinguished. The first is wild-type p63 that exists in heterozygous AEC patients. Due to the ability to form tetramers through the tetramerization domain, mutant p63 can form complexes with wild-type p63. Formation of aggregates by the mutant protein also draws wild-type p63 into larger aggregates, thus exerting a dominant negative effect. This effect was confirmed in our experiments by showing that mutant p63 in L514F heterozygous keratinocytes acts as a dominant negative inhibitor of wild-type p63 function. The second category includes other p63 binding partners. One example is the family member p73, which can form heterotetramers with p63, consisting of one p63 dimer and one p73 dimer. Structural studies have shown that p63/p73 heterotetramers are thermodynamically more stable than either homotetramer (49). Although the function of p63/p73 interactions in skin biology remains uncharacterized, both proteins are expressed simultaneously in the basal layer of the epidermis. While p63 is abundant in all cells, p73 is more highly expressed in the frequently dividing stem cell population (49, 50). The third category includes proteins that normally do not interact or interact very weakly with wild-type p63 but, due to the existence of hydrophobic patches, can coaggregate with aggregating mutant p63. One example is p53R175H, a structural mutant with gain-of-function properties that interacts with specific isoforms of p73 and, to a lesser extent, of p63, interfering with their functions (32, 51, 52). The p53R175H mutant interacts very weakly with wild type ΔNp63α (refs. 32 and 51 and present study), whereas it interacts strongly with AEC mutants. The biological significance of this interaction remains to be determined. Since p63 is an abundantly expressed transcription factor in keratinocytes, and AEC mutants often show a longer half-life in cells than the wild-type protein (36), mutant

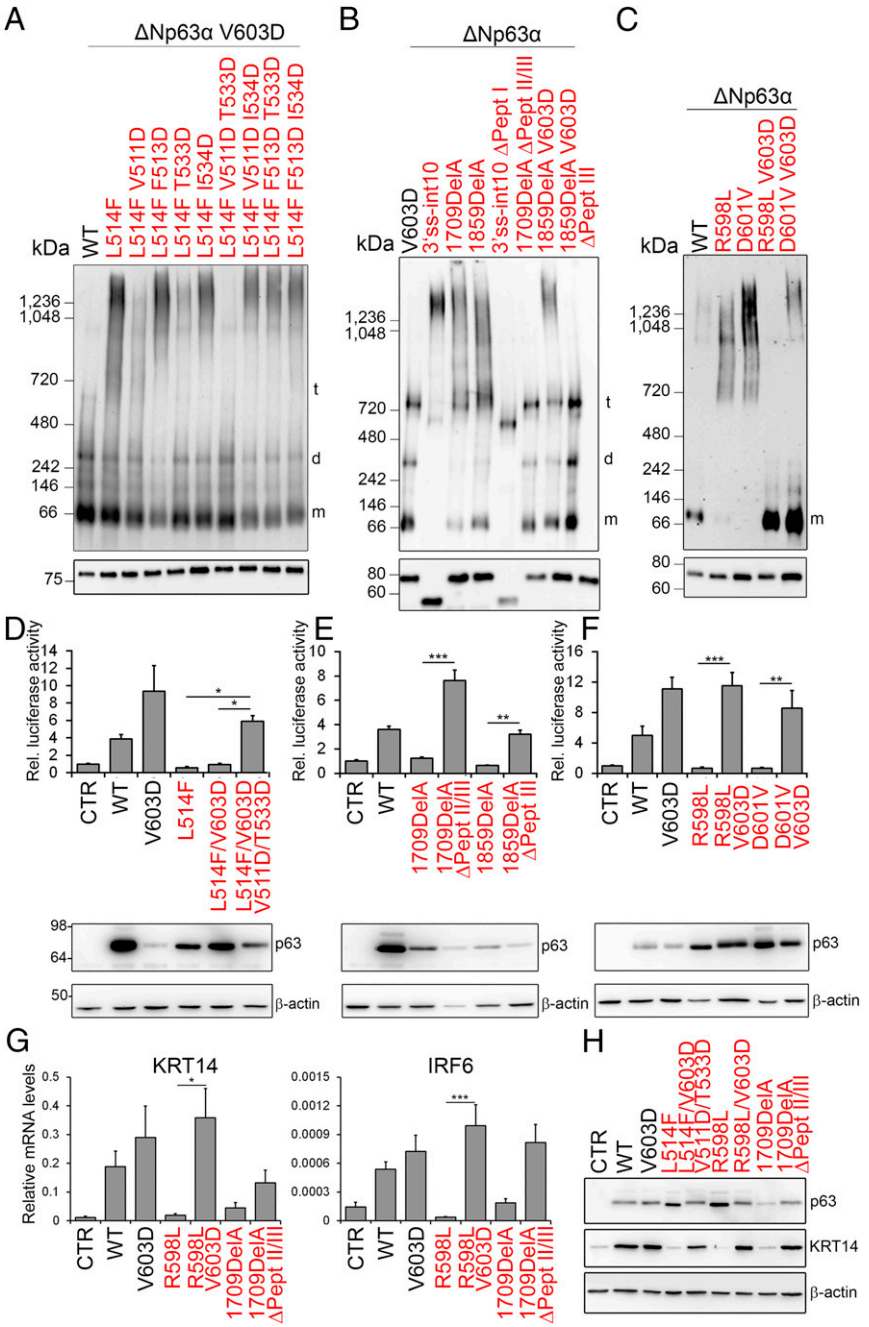

Fig. 5. Transcriptional activity is restored by reducing the aggregation propensity of AEC-associated mutant p63. (*A–C*) BN-PAGE (*Upper*) and SDS/PAGE (*Lower*) followed by Western blot of p63 and the indicated mutations and deletions transfected in HEK 293 cells. (*D–F*) Luciferase reporter assays of wild-type and mutant p63 on the KRT14 promoter in HEK293 cells ($n = 3$) (*Upper*). Luciferase data were normalized for *Renilla* luciferase activity. SDS/PAGE (*Lower*) followed by Western blot of wild-type and mutant p63 are shown as control. (*G*) Real-time RT-PCR of the indicated keratinocyte-specific p63 target genes in HDFs converted to iKCs by coinfection with KLF4 and the indicated p63 viruses. (*H*) Western blot of KRT14 and p63 in iKCs. β-actin was used as loading control. Data are shown as mean ± SEM, and statistical significance was assessed using one-way ANOVA analysis. $*P \leq 0.05$; $**P \leq 0.001$; $***P \leq 0.0001$.

p63 may be able to sequester other nuclear proteins. Aggregation between AEC mutants and p73 and/or other p63 protein partners helps explain the severe skin phenotype specifically observed in AEC syndrome and not in other diseases associated with p63 mutations. Future studies should focus on identifying nuclear proteins that may form large, inactive complexes with mutant p63. By revealing that AEC syndrome is a protein aggregation disorder and that aggregation can be reverted leading to a functional rescue, our studies open avenues for therapeutic intervention.

Materials and Methods

Detailed descriptions are provided in *SI Appendix*.

Mice. K14-Cre (Krt14-CreΔneo) knock-in mice were obtained from J. Huelsken, Swiss Institute for Experimental Cancer Research, Lausanne, Switzerland, and were used to induce expression of the p63 mutant protein in stratified epithelia at late stages of embryonic development (43). See *SI Appendix* for the conditional knock-in mice ($p63^{+/L514Fflox}$) generation. All mouse work was conducted at CEINGE according to the Italian ethical regulations under the animal license 311/2016-PR.

Coimmunoprecipitation, SDS/PAGE, BN-PAGE. For coimmunoprecipitation, cells were lysed in RIPA lysis buffer [20 mM Tris·HCl (pH 7.5), 150 mM NaCl, 1 mM Na_2EDTA, 1 mM EGTA, 1% Nonidet P-40, 1% sodium deoxycholate, 1 mM DTT] with the addition of protease and phosphatase inhibitors. Lysates were cleared by centrifugation and incubated with 2 μg of HA-antibody, p73 antibody, or normal IgG overnight at 4 °C. The immunocomplexes were purified with 25 μL of Protein G Dynabeads (Thermo Fisher Scientific) for 3 h at 4 °C. For SDS/PAGE, cells were loaded in Laemmli sample buffer with 5% β-mercaptoethanol. For BN-PAGE, cells were lysed in native lysis buffer [25 mM Tris (pH 7.5), 150 mM NaCl, 2 mM $MgCl_2$, 20 mM CHAPS, 1 mM DTT and protease inhibitors]. Collected cells were incubated 1 h on ice in the presence of benzonase (Merck Millipore). Protein extracts were then mixed with 20% Glycerol and 5 mM Coomassie G-250 and loaded on 3–12% Novex Bis-Tris gradient gel for BN-PAGE (Thermo Fisher Scientific). Antibodies used in this study are listed in *SI Appendix*, Table S5.

Analytical SEC. Analytical SEC experiments were performed as previously described (9, 32). Briefly, either a Superose 6 PC 3.2/300 column (GE Healthcare) for in vitro translated p63 or a Superose 6 GL 10/300 column (GE Healthcare) for cell lysates of transiently transfected H1299 cells were used. H1299 cell lysate was prepared by three cycles of freezing and thawing in SEC running buffer (50 mM Tris pH 7.5; 150 mM NaCl; 1 mM DTT) with protease inhibitors and Benzonase followed by removal of cell debris by centrifugation. Before injection, cell lysates were incubated at 37 °C for 15 min. The Superose 6 GL 10/300 column was calibrated using the Gel Filtration HMW and LMW Calibration Kits.

RNA Isolation, RT-qPCR, and ChIP-qPCR. For RT-qPCR, total RNA was extracted using TRIzol reagent (Thermo Fisher Scientific) and cDNA was synthesized using SuperScript Vilo, Real time RT-PCR was performed using the SYBR Green PCR master mix (Thermo Fisher Scientific) in an ABI PRISM 7500 (Thermo Fisher Scientific). Target genes were quantified using specific oligonucleotide primers (*SI Appendix*, Table S4) and normalized for mouse β-actin or human RPLP0 expression. For ChIP-qPCR, chromatin was immunoprecipitated as previously reported (44). Immunoprecipitation was performed using rabbit antibodies for p63 or rabbit IgG as control. Bound chromatin was purified with Protein A Sepharose (GE Healthcare) for 1 h at 4 °C. Bound DNA was quantified by real-time PCR using specific oligonucleotide primers (*SI Appendix*, Table S4) and normalized to input.

CD Melting Curve. CD melting curves of p63 SAM or L514F mutant were recorded with Jasco J-810 spectropolarimeter (Jasco Labortechnik). Changes in CD signal at 222 nm and dynode voltage were recorded from 20 °C to 95 °C and backward from 95 °C to 20 °C. Melting curves were corrected for the pretransition phase and melting points were acquired using the Boltzman sigmoidal fit function (Origin Pro-9.1G). To follow turbidity as an indicator of precipitation and aggregation during unfolding, the dynode voltage was plotted against the temperature as described before (53).

DNA Pulldown Assay. Oligonucleotides used for the DNA pulldown assay correspond to the p53/p63/p73 binding site on the CDKN1A promoter (9). Biotinylated annealed DNA strands were immobilized on streptavidin agarose beads (GE Healthcare) in pulldown buffer (50 mM Tris pH 8.0; 150 mM NaCl; 0.1% Tween-20), incubated with in vitro translated p63 and washed four times with pulldown buffer. Bound p63 was eluted with boiling sample buffer and pulldown efficiency was analyzed by Western blot.

NMR Spectroscopy and Structure Determination. All spectra were recorded at 296 K on Bruker Avance spectrometers (proton frequencies of 600 MHz and 800 MHz) equipped with cryo-probes. The NMR structure of the murine p63 SAM L514F mutant was obtained using combined automated NOE assignment and structure calculation (54) with the program package CYANA (55). An overview of the structural statistics is given in *SI Appendix*, Table S1. Details about the recorded spectra and structure calculation are described in *SI Appendix*. The accession number for the coordinates and structures factors of murine p63 SAM L514F mutant reported in this manuscript is PDB ID code 5N2O.

Quantification and Statistical Analysis. All datasets derive from at least three independent experiments unless otherwise indicated. The number of independent experiments are indicated (*n*), with the exception of Fig. 3*J* in which *n* indicate number of analyzed animals. Data are presented as the mean of independent experiments ±SEM or SD as indicated. All statistical analyses were performed using GraphPad Prism software (version 7.0). In experiments comparing two samples, paired or unpaired, two-tailed *t* testing was performed, whereas when comparing multiple independent samples, one-way analysis of variance (ANOVA) followed by Tukey's HSD multiple comparison post hoc tests were performed as described in the figure legends. *P* values of statistical significance are represented as $*P \leq 0.05$; $**P \leq 0.01$; $***P \leq 0.001$.

ACKNOWLEDGMENTS. We thank Anna Mandinova for critical reading of the manuscript and helpful discussion; George Sen for helpful discussion on the HDF-to-iKC conversion assay; Eleonora Candi, Bert Vogelstein, and Adele Abbate (Reithera Srl) for reagents; Dario Acampora (Institute of Genetics and Biophysics "A. Buzzati Traverso") for generating mice; Annamaria Carissimo and the Telethon Institute of Genetics and Medicine Bioinformatics Core for assistance in the statistical analysis; and Maria Rosaria Mollo for the initial mouse characterization. We appreciate language and content editing assistance provided by DerMEDit. This work was supported by Telethon Grants GGP09230 and GGP16235 (to C.M.), ERA-Net Research Program on Rare Diseases (ERARE-2) Skin-Dev (C.M.), Italian Association for Cancer Research Grant IG2011-N.11369 (to C.M.), Fondation Dind-Cottier pour la recherche sur la peau (C.M.), DFG Grant DO 545/8-1 (to V.D.), the Centre for Biomolecular Magnetic Resonance, and the Cluster of Excellence Frankfurt (Macromolecular Complexes). P.G. is supported by a Lichtenberg Professorship of the Volkswagen Foundation. C.R. is a PhD student in molecular oncology at the European School of Molecular Medicine.

1. Koster MI, Kim S, Mills AA, DeMayo FJ, Roop DR (2004) p63 is the molecular switch for initiation of an epithelial stratification program. *Genes Dev* 18:126–131.
2. Mills AA, et al. (1999) p63 is a p53 homologue required for limb and epidermal morphogenesis. *Nature* 398:708–713.
3. Nguyen BC, et al. (2006) Cross-regulation between Notch and p63 in keratinocyte commitment to differentiation. *Genes Dev* 20:1028–1042.
4. Senoo M, Pinto F, Crum CP, McKeon F (2007) p63 Is essential for the proliferative potential of stem cells in stratified epithelia. *Cell* 129:523–536.
5. Truong AB, Kretz M, Ridky TW, Kimmel R, Khavari PA (2006) p63 regulates proliferation and differentiation of developmentally mature keratinocytes. *Genes Dev* 20:3185–3197.
6. Yang A, et al. (1999) p63 is essential for regenerative proliferation in limb, craniofacial and epithelial development. *Nature* 398:714–718.
7. Vanbokhoven H, Melino G, Candi E, Declercq W (2011) p63, a story of mice and men. *J Invest Dermatol* 131:1196–1207.
8. Yang A, et al. (1998) p63, a p53 homolog at 3q27-29, encodes multiple products with transactivating, death-inducing, and dominant-negative activities. *Mol Cell* 2:305–316.
9. Deutsch GB, et al. (2011) DNA damage in oocytes induces a switch of the quality control factor TAp63α from dimer to tetramer. *Cell* 144:566–576.
10. Coutandin D, et al. (2009) Conformational stability and activity of p73 require a second helix in the tetramerization domain. *Cell Death Differ* 16:1582–1589.
11. Rocco JW, Leong CO, Kuperwasser N, DeYoung MP, Ellisen LW (2006) p63 mediates survival in squamous cell carcinoma by suppression of p73-dependent apoptosis. *Cancer Cell* 9:45–56.
12. Suh EK, et al. (2006) p63 protects the female germ line during meiotic arrest. *Nature* 444:624–628.
13. Crum CP, McKeon FD (2010) p63 in epithelial survival, germ cell surveillance, and neoplasia. *Annu Rev Pathol* 5:349–371.
14. Ferone G, et al. (2013) p63 control of desmosome gene expression and adhesion is compromised in AEC syndrome. *Hum Mol Genet* 22:531–543.
15. Ferone G, et al. (2012) Mutant p63 causes defective expansion of ectodermal progenitor cells and impaired FGF signalling in AEC syndrome. *EMBO Mol Med* 4:192–205.
16. Antonini D, et al. (2010) Transcriptional repression of miR-34 family contributes to p63-mediated cell cycle progression in epidermal cells. *J Invest Dermatol* 130:1249–1257.
17. De Rosa L, et al. (2009) p63 Suppresses non-epidermal lineage markers in a bone morphogenetic protein-dependent manner via repression of Smad7. *J Biol Chem* 284:30574–30582.
18. LeBoeuf M, et al. (2010) Hdac1 and Hdac2 act redundantly to control p63 and p53 functions in epidermal progenitor cells. *Dev Cell* 19:807–818.
19. Ramsey MR, He L, Forster N, Ory B, Ellisen LW (2011) Physical association of HDAC1 and HDAC2 with p63 mediates transcriptional repression and tumor maintenance in squamous cell carcinoma. *Cancer Res* 71:4373–4379.
20. Cicero DO, et al. (2006) NMR structure of the p63 SAM domain and dynamical properties of G534V and T537P pathological mutants, identified in the AEC syndrome. *Cell Biochem Biophys* 44:475–489.
21. McGrath JA, et al. (2001) Hay-Wells syndrome is caused by heterozygous missense mutations in the SAM domain of p63. *Hum Mol Genet* 10:221–229.
22. Chi SW, Ayed A, Arrowsmith CH (1999) Solution structure of a conserved C-terminal domain of p73 with structural homology to the SAM domain. *EMBO J* 18:4438–4445.
23. Coutandin D, et al. (2016) Quality control in oocytes by p63 is based on a spring-loaded activation mechanism on the molecular and cellular level. *Elife* 5:e13909.
24. Straub WE, et al. (2010) The C-terminus of p63 contains multiple regulatory elements with different functions. *Cell Death Dis* 1:e5.

25. Rinne T, Hamel B, van Bokhoven H, Brunner HG (2006) Pattern of p63 mutations and their phenotypes–Update. *Am J Med Genet A* 140:1396–1406.
26. Celli J, et al. (1999) Heterozygous germline mutations in the p53 homolog p63 are the cause of EEC syndrome. *Cell* 99:143–153.
27. Julapalli MR, Scher RK, Sybert VP, Siegfried EC, Bree AF (2009) Dermatologic findings of ankyloblepharon-ectodermal defects-cleft lip/palate (AEC) syndrome. *Am J Med Genet A* 149A:1900–1906.
28. Ianakiev P, et al. (2000) Split-hand/split-foot malformation is caused by mutations in the p63 gene on 3q27. *Am J Hum Genet* 67:59–66.
29. Payne AS, et al. (2005) Two novel TP63 mutations associated with the ankyloblepharon, ectodermal defects, and cleft lip and palate syndrome: A skin fragility phenotype. *Arch Dermatol* 141:1567–1573.
30. Sathyamurthy A, Freund SM, Johnson CM, Allen MD, Bycroft M (2011) Structural basis of p63α SAM domain mutants involved in AEC syndrome. *FEBS J* 278:2680–2688.
31. Fernandez-Escamilla AM, Rousseau F, Schymkowitz J, Serrano L (2004) Prediction of sequence-dependent and mutational effects on the aggregation of peptides and proteins. *Nat Biotechnol* 22:1302–1306.
32. Kehrloesser S, et al. (2016) Intrinsic aggregation propensity of the p63 and p73 TI domains correlates with p53R175H interaction and suggests further significance of aggregation events in the p53 family. *Cell Death Differ* 23:1952–1960.
33. Xu J, et al. (2011) Gain of function of mutant p53 by coaggregation with multiple tumor suppressors. *Nat Chem Biol* 7:285–295.
34. Candi E, et al. (2007) DeltaNp63 regulates thymic development through enhanced expression of FgfR2 and Jag2. *Proc Natl Acad Sci USA* 104:11999–12004.
35. Romano RA, Birkaya B, Sinha S (2007) A functional enhancer of keratin14 is a direct transcriptional target of deltaNp63. *J Invest Dermatol* 127:1175–1186.
36. Browne G, et al. (2011) Differential altered stability and transcriptional activity of ΔNp63 mutants in distinct ectodermal dysplasias. *J Cell Sci* 124:2200–2207.
37. Chen Y, Mistry DS, Sen GL (2014) Highly rapid and efficient conversion of human fibroblasts to keratinocyte-like cells. *J Invest Dermatol* 134:335–344.
38. Ingraham CR, et al. (2006) Abnormal skin, limb and craniofacial morphogenesis in mice deficient for interferon regulatory factor 6 (Irf6). *Nat Genet* 38:1335–1340.
39. Richardson RJ, et al. (2006) Irf6 is a key determinant of the keratinocyte proliferation-differentiation switch. *Nat Genet* 38:1329–1334.
40. Thomason HA, et al. (2010) Cooperation between the transcription factors p63 and IRF6 is essential to prevent cleft palate in mice. *J Clin Invest* 120:1561–1569.
41. Petiot A, et al. (2003) A crucial role for Fgfr2-IIIb signalling in epidermal development and hair follicle patterning. *Development* 130:5493–5501.
42. Romano RA, Ortt K, Birkaya B, Smalley K, Sinha S (2009) An active role of the DeltaN isoform of p63 in regulating basal keratin genes K5 and K14 and directing epidermal cell fate. *PLoS One* 4:e5623.
43. Huelsken J, Vogel R, Erdmann B, Cotsarelis G, Birchmeier W (2001) beta-Catenin controls hair follicle morphogenesis and stem cell differentiation in the skin. *Cell* 105:533–545.
44. Antonini D, et al. (2015) A composite enhancer regulates p63 gene expression in epidermal morphogenesis and in keratinocyte differentiation by multiple mechanisms. *Nucleic Acids Res* 43:862–874.
45. Kouwenhoven EN, et al. (2010) Genome-wide profiling of p63 DNA-binding sites identifies an element that regulates gene expression during limb development in the 7q21 SHFM1 locus. *PLoS Genet* 6:e1001065.
46. Rinne T, Bolat E, Meijer R, Scheffer H, van Bokhoven H (2009) Spectrum of p63 mutations in a selected patient cohort affected with ankyloblepharon-ectodermal defects-cleft lip/palate syndrome (AEC). *Am J Med Genet A* 149A:1948–1951.
47. Bertola DR, et al. (2004) Molecular evidence that AEC syndrome and Rapp-Hodgkin syndrome are variable expression of a single genetic disorder. *Clin Genet* 66:79–80.
48. Clements SE, et al. (2010) Rapp-Hodgkin and Hay-Wells ectodermal dysplasia syndromes represent a variable spectrum of the same genetic disorder. *Br J Dermatol* 163:624–629.
49. Gebel J, et al. (2016) Mechanism of TAp73 inhibition by ΔNp63 and structural basis of p63/p73 hetero-tetramerization. *Cell Death Differ* 23:1930–1940.
50. Sada A, et al. (2016) Defining the cellular lineage hierarchy in the interfollicular epidermis of adult skin. *Nat Cell Biol* 18:619–631.
51. Gaiddon C, Lokshin M, Ahn J, Zhang T, Prives C (2001) A subset of tumor-derived mutant forms of p53 down-regulate p63 and p73 through a direct interaction with the p53 core domain. *Mol Cell Biol* 21:1874–1887.
52. Lang GA, et al. (2004) Gain of function of a p53 hot spot mutation in a mouse model of Li-Fraumeni syndrome. *Cell* 119:861–872.
53. Benjwal S, Verma S, Rohm KH, Gursky O (2006) Monitoring protein aggregation during thermal unfolding in circular dichroism experiments. *Protein Sci* 15:635–639.
54. Güntert P, Buchner L (2015) Combined automated NOE assignment and structure calculation with CYANA. *J Biomol NMR* 62:453–471.
55. Güntert P, Mumenthaler C, Wüthrich K (1997) Torsion angle dynamics for NMR structure calculation with the new program DYANA. *J Mol Biol* 273:283–298.

SI Appendix (Russo et al.)

Materials and Methods

Cell Culture

Primary mouse keratinocytes were isolated from newborn skin as described (1) and cultured under low calcium condition (0.05mM) in 4% calcium-chelated Fetal Bovine Serum (FBS) (Thermo Fisher Scientific) and Epidermal Growth Factor (EGF) (Thermo Fisher Scientific). Neonatal HDFn (Thermo Fisher Scientific), HEK293, H1299 and Saos-2 were grown in Dulbecco's Modified Eagle Medium (DMEM) and 10% FBS (Thermo Fisher Scientific).

Plasmids, transfections and luciferase assay

All *p63* mutant constructs were obtained using the QuikChange site-directed mutagenesis kit (Agilent) starting from either pCMV2-FLAG-mΔNp63α or pcDNA3.1-Myc-hΔNp63α using mutagenesis primers (Table S4). For HDF to iKC conversion, wild type p63 and its mutants were cloned in pBABE in the BamHI site. Cells were transfected using Lipofectamine 2000 (Thermo Fisher Scientific). Luciferase activity was determined 48 hr after transfection using the dual-luciferase reporter assay kit (Promega). pKRT14 promoter-luc (2), pG13-luc (3), and pFGFR2 enhancer-luc (1) were used as reporters. Renilla activity was used to normalize transfection efficiency. For *E. coli* expression of the murine wild-type and mutant p63 SAM domains see Supplementary Information.

Adenoviral infection and retroviral infection

Mouse primary keratinocytes were infected 5 days after plating with adenovirus carrying GFP as control or Cre recombinase at MOI 100 for 2 hr in low calcium medium without serum and EGF. Cells were collected four days after infection. High titer retroviral production was obtained in HEK293T cells by transient transfection of the pBABE constructs and of amphotropic viral envelope plasmid (pAmpho) using Lipofectamine 2000 (Thermo Fisher Scientific) as described (4). Cell supernatants containing the retroviruses were collected 48 and 72 hr after transfection. Neonatal HDF were infected twice at 20-30% confluence with retroviruses carrying p63 and KLF4 (5) in the presence of 8 μg/ml Polybrene. Cells were passage, selected with 2 μg/ml puromycin 48 hr after the second infections, and grown after 48 hr of selection for 15-18 days in the absence of puromycin as previously described (6).

Generation of the L514F conditional knock-in construct

A genomic portion of the mouse *p63* gene (16265bp) from exon 12 to the 3'UTR derived from the bMQ-241L2 BAC clone was subcloned into NotI and SpeI restriction site of pL253 vector via gap repair (7). Miniarms were cloned into the NotI and SpeI sites of pL253 using Ap63CDNU and Ap63CDNL, or Bp63CDNU and Bp63CDNL oligonucleotide primers. The PCR products were digested with NotI and HindIII (Ap63CDNU/L), or HindIII and SpeI (Bp63CDNU/L) respectively. The vector was subsequently linearized with HindIII and electroporated into the recombinogenic bacterial strain EL350 containing the bMQ-241L2 BAC clone to obtain the pL253-p63 plasmid. To insert a first LoxP site 400bp upstream of exon 13, miniarms (PCR product: CmP63U-CmP63L and DmP63U-DmP63L) were cloned into NotI-EcoRI or BamHI-SalI sites in the pL452 vector (7) containing the PGK-Neo cassette flanked by LoxP sites. The "armed" PGK-Neo cassette and pL253-P63 were co-electroporated into the recombinogenic bacterial strain EL350. PGK-Neo cassette was excised by Cre-recombinase to obtain pL253-P63Lox1 plasmid. Two unique restriction enzyme sites (ISceI and ICeuI) flanking Blasticidin (Bsd) were inserted in the pL253-p63Lox1 plasmid to substitute exon 14. Miniarms (PCR product: C1mP63U-C1mP63L and D1mP63U-D1mP63L) were cloned into NotI-

EcoRI or BamHI-SalI sites in the the pBS I-SceI-Bsd-I-CeuI vector. The "armed" I-SceI-Bsd-I-CeuI cassette was co-electroporated with the pL253-P63Lox1 plasmid into the bacterial strain EL350 to obtain the pL253-P63Lox1-Bsd plasmid.

To insert 3xFlag tag in the p63 exon 14, genomic DNA was amplified with P63ex14fgU-P63ex14fgL, and the PCR product was digested with EcoRI and SmaI to insert in BamHI (filled) - KpnI sites of p3xFlag-CMV-14-C (Sigma). p63 exon 14 -3xFlag was amplified from p3xFlag-CMV-p63ex14 using ISceIE14U and ICeuIFlagL oligonucleotides and cloned into ISceI and ICeuI restriction sites of pL253-P63Lox1-Bsd to generate pL253-P63Lox1-Ex14-3xFlag.

Subsequently, genomic DNA was amplified with DmP63U2, Ex13L2 oligonucleotides and cDNA with Ex13U2, RecEx14L3 oligonucleotides to generate a DNA fragment containing p63 exons 13 and 14 fused by recombinant PCR. At the same time, mutant p63 exon 13 (L514F) was generated by recombinant PCR using DmP63U, Ex13MutL, Ex13MutU, RecEx13L oligonucleotides. These 2 DNA fragments were inserted respectively into NotI-EcoRI and BamHI-SalI restriction sites of pL451, to generate pL451 armed plasmid. Furthermore, 3 polyadenylation sites from pSA-Lox-Neo-tpA BamHI digested in BglII was inserted in the pL451armed. The plasmid was digested with NotI and SalI and the relevant fragment was electroporated with the plasmid pL253-P63Lox1-Ex14-3xFlag into the EL350 to generate the final construct including the recombination cassette (Fig.S3B). See Table S4 for the list of oligonucleotide primers described in this section.

Generation of the conditional knock-in L514F mutant mice

The p63L514F mutation was inserted into the p63 locus in E14TG2a (129/Ola) ES cells by homologous recombination using the recombination construct describe above linearized with NotI, essentially as previously described (1). Twenty-four hours after electroporation ES cells were selected with 100 µg/ml G418 (Thermo Fisher Scientific) for 7 days. Neo-resistant ES clones were screened at 3' and 5' for the correct insertion in the p63 endogenous locus by PCR analysis using the TaKaRa LA Taq® DNA Polymerase (Clontech) with an oligonucleotide annealing in the neomycin cassette and another on the genomic DNA (5'Arm Forward and Reverse; 3'Arm Forward and Reverse) (Figure S3C and Table S4). The homologous recombination event was also confirmed by Southern blotting (Figure S3D). Genomic DNA was digested with HindIII and analyzed with a probe located inside the neomycin cassette. An ES positive clone was injected into C57BL/6 blastocysts and the obtained chimeric mice were tested for germline transmission by breeding with C57BL/6 females. Offspring was genotyped for germline transmission of the p63L514F wild-type and mutant allele by PCR using tail genomic DNA and specific primers (L514F3xFlag For and L514F3xFlag Rev)) (Table S4). The neomycin cassette was removed by breeding the first generation of heterozygous mice with transgenic mice carrying the Flip recombinase. Mouse genotyping was performed by PCR with the indicated oligonucleotide primers (Table S4).

Protein Expression and Purification in *E. coli*

For *E. coli* expression of the murine p63 SAM L514F and subsequent structure determination by NMR, the mutant domain (amino acid 506-570) was subcloned into a pGEX-6P-2 expression vector (GE Healthcare) using the BamHI and XhoI restriction sites, and expressed in BL21(DE3)pLysS cells (Thermo Fisher Scientific). Unlabeled expression was carried out in 2xYT medium, while labeled expression was done in M9 minimal medium as described previously (8). Protein was expressed for 5hr at 23°C after induction with 1 mM IPTG, and cells were lysed by

sonification in PBS buffer supplemented with lysozyme (Sigma), DNAse (Sigma) and protease inhibitors. After centrifugation supernatant was loaded onto Glutathione Sepharose 4 Fast Flow Resin (GE Healthcare). Bound protein was washed with PBS and eluted with GST-elution buffer (50 mM Tris-HCl; 10 mM reduced glutathione; pH 8.0). Fractions containing protein were pooled and treated with Prescission-protease (GE Healthcare) for cleavage of the GST-tag. For removal of free GST and Prescission-Protease and concomitant buffer exchange cleaved protein was subjected to SEC on a Superdex 75 16/60 column (GE Healthcare) equilibrated in NMR Buffer (20 mM HEPES; 50 mM NaCl; 1 mM DTT; pH 7.0). Exchange of an unlabeled sample from H_2O to D_2O was achieved by several rounds of dilution and concentration with D_2O NMR Buffer. For concentration Amicon Centrifugal Filter Units were used (Merck Millipore).

For CD melting curve analysis of *E. coli* expressed protein, the human p63 SAM wild-type and L514F variant (amino acid 506-572) were subcloned into a pGEX-6p-2 expression vector, which was modified by substituting the PreScission-protease site with an 8xHis-tag followed by TEV-protease cleavage site, referred to as pGEX-6p-2-8xHis-TEV. The SAM domains were expressed in T7 Express cells (New England Biolabs) at 18°C overnight after induction with 1 mM IPTG. Cells were lysed by sonification in IMAC-A buffer (25 mM Tris; 200 mM NaCl; 25 mM Imidazole; pH 7.8) supplemented with lysozyme (Sigma), DNAse (Sigma) and protease inhibitors. After centrifugation the supernatant was applied on HisTrap columns (GE Healthcare). Bound protein was washed with IMAC-A buffer and eluted with IMAC-B buffer (25 mM Tris; 200 mM NaCl; 400 mM Imidazole; pH 7.8). Fractions containing protein were pooled and dialyzed in IMAC-A buffer after addition of His-tagged TEV-protease for cleavage of the GST-8xHis-tag. The cleaved tag and TEV-protease were removed by reverse IMAC purification. For final removal of impurities and concurrent exchange to CD Buffer (25mM HEPES; 100mM NaCl; 1mM DTT; pH 7.5) protein was further purified using a Superdex 75 16/60 column.

NMR Spectroscopy and structure Determination

For the backbone assignment a 3D HNCACB spectrum was used. Aliphatic and aromatic side chains were assigned with 3D [^{15}N,^{1}H]-TOCSY-HSQC, [^{15}N,^{1}H]-NOESY-HSQC (in H_2O) and 2D NOESY (in D_2O) spectra. Distance restraints were derived from [^{15}N,^{1}H]-NOESY-HSQC (in H_2O) and 2D NOESY (in D_2O) spectra.

The NMR structure of the murine p63 SAM L514F mutant was obtained using combined automated NOE assignment and structure calculation (9) with the program package CYANA (10). As input for CYANA, peak lists from [^{15}N,^{1}H]-NOESY-HSQC in H_2O and homonuclear NOESY in D_2O, the manual established chemical shift assignment, dihedral angle restraints obtained from chemical shift analysis by Talos+ (11), hydrogen bond restraints and the amino acid sequence were used. The structure calculation was performed using 200 random starting conformers and 10,000 torsion angle dynamic steps. All remaining parameters were kept at their default values. The 20 conformers with the lowest CYANA target function values were used for represent the solution structure. Restrained energy refinement was conducted using OPALp (12), which relies on the AMBER force field (13). An overview of the structural statistics is given in SI Appendix, Table S1.

Electrophoretic Mobility Shift Assay (EMSA)

After transfection with the indicated p63 wild-type or mutants expressing constructs, nuclear extracts from HEK293 cells were prepared, and EMSA was performed as described (14). Oligonucleotide primer used for EMSA correspond to the KRT14 enhancer site (14). The protein–DNA complexes

were resolved by gel electrophoresis on 5% non-denaturing polyacrylamide gels, dried and visualized by autoradiography.

SI Figures

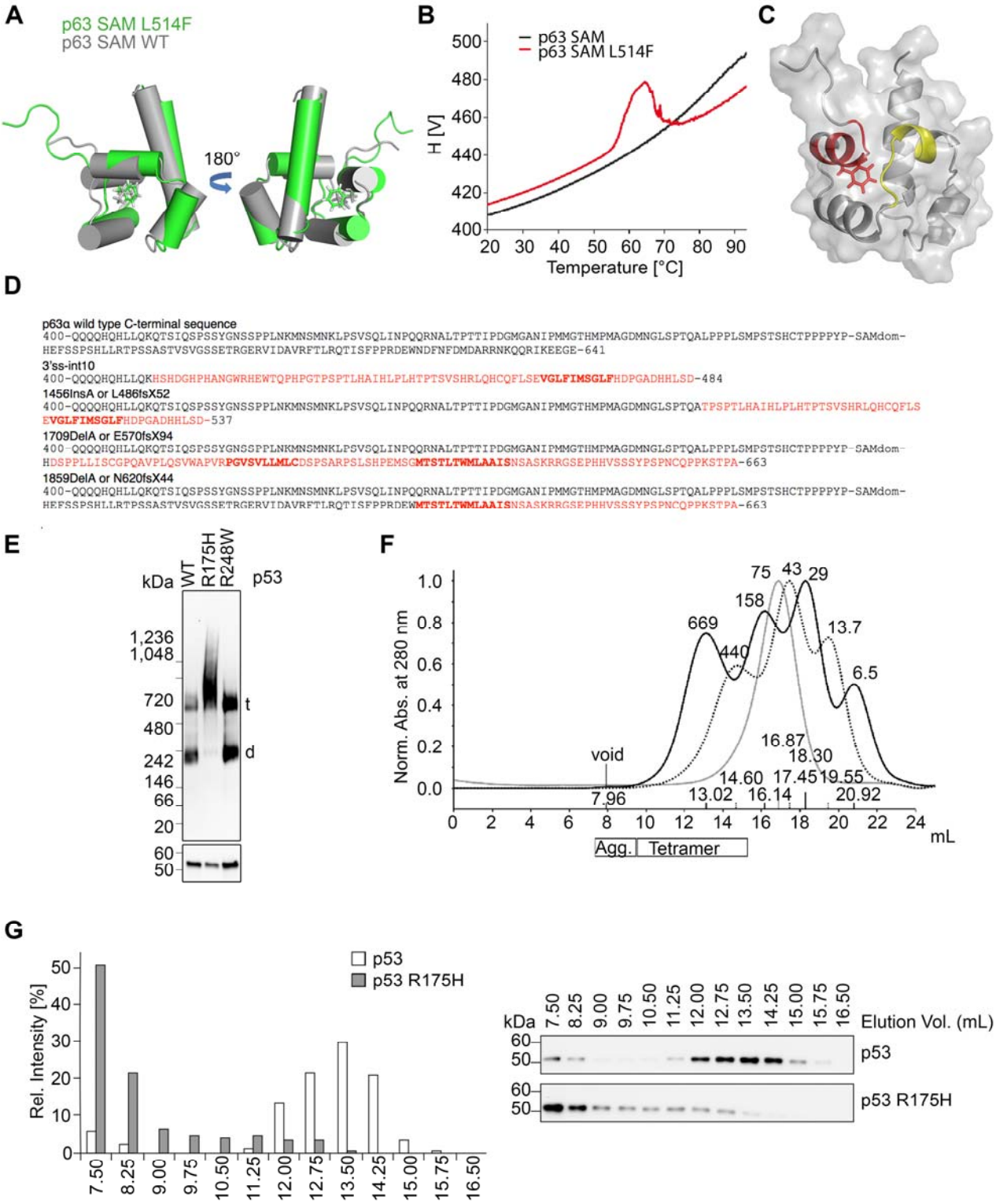

Figure S1. Aggregation propensity of mutant p63L514F

A. A representative conformer of the NMR structure of the murine p63L514F SAM (green) was superimposed with the wild type p63 SAM structure (grey; PDB: 1RG6). Amino acids L514 and F514 are depicted as sticks in their respective color.

B. Sample turbidity of wild type p63 SAM (black) and p63L514F SAM (red) as measurement of precipitation and aggregation upon unfolding during the CD melting experiment (15). Dynode voltage: H[V])

C. The two aggregation prone segments of the p63 SAM domain, a.a. 508-515 (red) and a.a. 530-537 (yellow), were mapped on the NMR structure of the L514F mutant. F514 is highlighted as sticks.
D. C-terminal sequence of wild type p63α and its frameshift mutations causative of AEC syndrome. The SAM domain sequence is indicated as -*SAMdomain*-. Amino acid generated by frameshift are indicated in red. Sequences with an aggregation propensity are indicated in bold.
E. BN-PAGE and Western blot for p53 in H1299 extracts expressing wild type p53 and two cancer mutations R175H, known to cause aggregation, and R248W that has lost the DNA binding ability. P53 run as dimer (d) and tetramer (t). SDS-PAGE as control of p53 loading is in the lower panel.
F. The Superose 6 GL 10/300 column used for SEC analysis of H1299 cell lysate was calibrated using molecular weight standards. Protein standards are expressed in kDa above the peak and the precise elution volume is on the x-axis.
G. SEC followed by Western blot of H1299 cell lysates overexpressing wild type p53 and the mutant p53R175H. Samples were incubated at 37°C for 15 min. before loading on SEC. Bar diagrams show the relative intensities of each collected fraction.

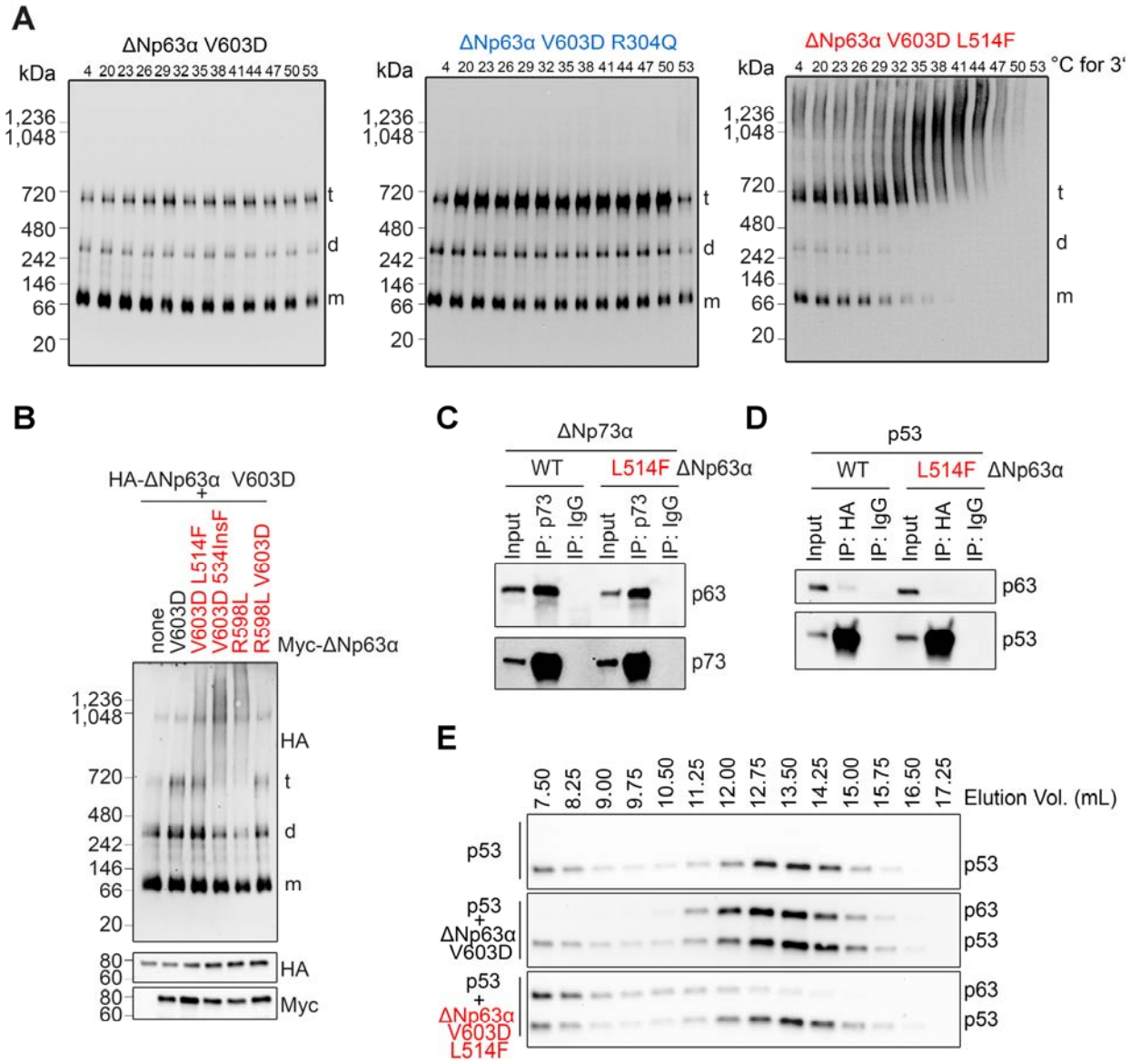

Figure S2. AEC-associated p63 mutants form aggregates with wild type p63 and others p53 family members.

A. BN-PAGE coupled with a cellular thermal shift assay (CETSA) (16) to test wild type and mutant p63 thermodynamic stability in cell lysate of H1299 cells. Soluble ΔNp63α protein ran mainly as a monomer (m) and tetramer (t) with a minor dimeric (d) population. Aggregates migrated at sizes above the tetramer.

B. BN-PAGE of co-expressed HA-tagged ΔNp63α V603D with Myc-tagged wild type or mutant p63 in H1299 cells. Immunoblot were revealed with anti-Myc or anti-Ha as indicated. SDS-PAGE as control of p63 loading is in the lower panel.

C. Co-immunoprecipitation experiment of Myc-tagged ΔNp63α wild type or L514F with ΔNp73α in H1299 cells and Western blot with the indicated antibodies.

D. Co-immunoprecipitation between wild type HA-p53 and the indicated Myc-ΔNp63α proteins. p53 was immunoprecipitated (IP) with an HA-specific antibody and detected with HA for p53, or Myc for p63.

E. SEC analysis and Western blot of p53 alone or co-expressed with ΔNp63αV603D either wild type or L514F in H1299 cells.

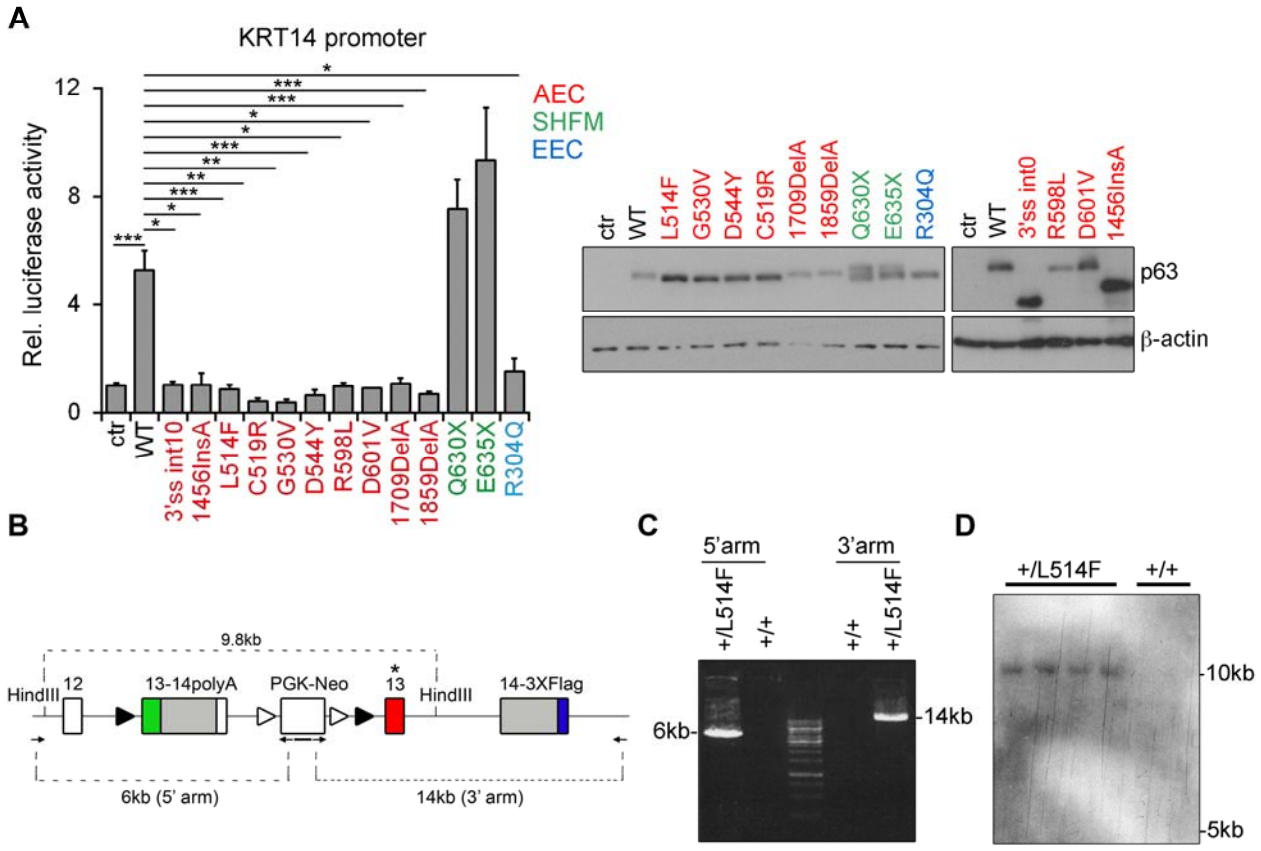

Figure S3. Transcriptional activity of wild type and mutant p63 and gene targeting strategy for the p63+/floxL514F knock-in ES cells.

A. Luciferase reporter assay (left panel) and SDS-PAGE (right panel) followed by Western blot of wild type and mutant p63 on the KRT14 promoter in HEK293 cells. β-actin was used as loading control. Data were normalized for *Renilla* luciferase activity (n=11). Data are shown as mean ± SEM and statistical significance was assessed using one-way ANOVA analysis. * $p \leq 0.05$; **; $p \leq 0.001$; ***$p \leq 0.0001$.

B. Schematic representation of the gene targeting vector used to generate the inducible p63L514F knock-in mice. The targeted locus is depicted as in Fig. 3C. The upper dotted black line indicates the fragment generated by the knock-in allele upon HindIII digestion performed in S3D. The lower dotted black lines indicate the fragments generated by PCR performed in S3C. Oligonucleotide primers (arrows, see Table S4) used for PCR analysis and the relative PCR product length are indicated.

C. PCR analysis performed on genomic DNA derived from the ES cell clone used to generate the knock-in mouse using specific oligonucleotide primers (see Table S4) in order to confirm the insertion of 5' arm and 3' arm respectively.

D. Southern blot analysis of genomic DNA derived from several ES cell clones digested with HindIII and probed with a neomycin-specific fragment (1).

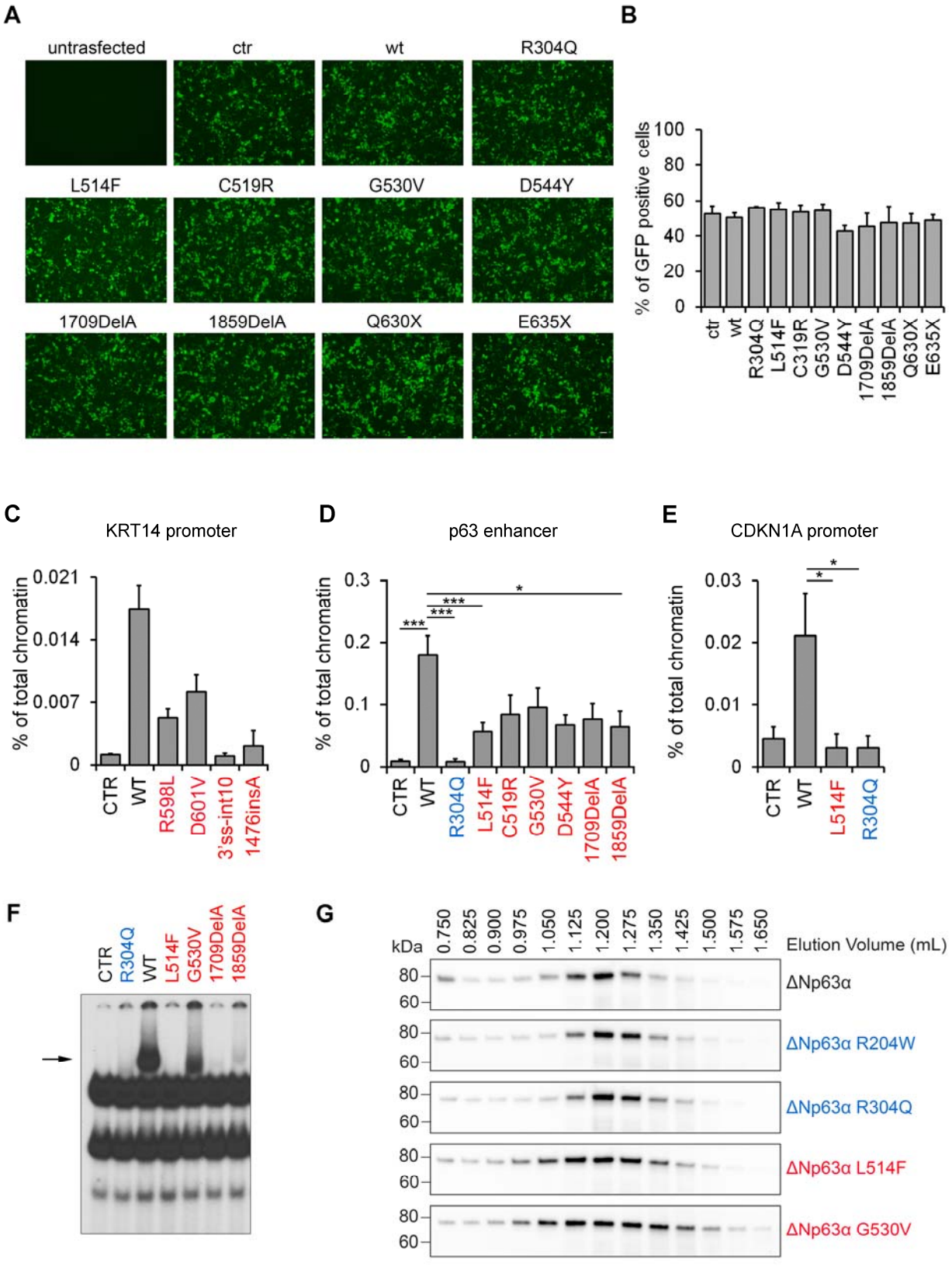

Figure S4. AEC-associated p63 mutants exhibit impaired DNA binding in cells.
A. Representative fluorescent GFP signal in HEK293 co-transfected with wild type or mutant p63 and pEGFP-C1 (Clontech) used as transfection control.
B. Quantification of GFP positive cells of the experiment in A using ImageJ software. Data are shown as mean ± SD, n=2.

C-E. ChIP-qPCR analysis in HEK293 cells overexpressing wild type and mutant p63 on the KRT14 and CDKN1A promoters (n=2, n=5 respectively), and of the p63 enhancer (n=18).
F. EMSA in HEK293 nuclear extracts of the indicated wild type and mutant p63 proteins with a radiolabeled probe corresponding to the KRT14 promoter sequence.
G. SEC analysis and Western blot of *in vitro* translated p63 proteins. Wild type and mutant p63 proteins eluted as a tetrameric protein with no signal in the aggregation fraction (0.75 ml).
Data are shown as mean ± SEM with the exception of (C) in which error bars indicate SD. Statistical significance was assessed using one-way ANOVA analysis. * $p \leq 0.05$; ***$p \leq 0.0001$.

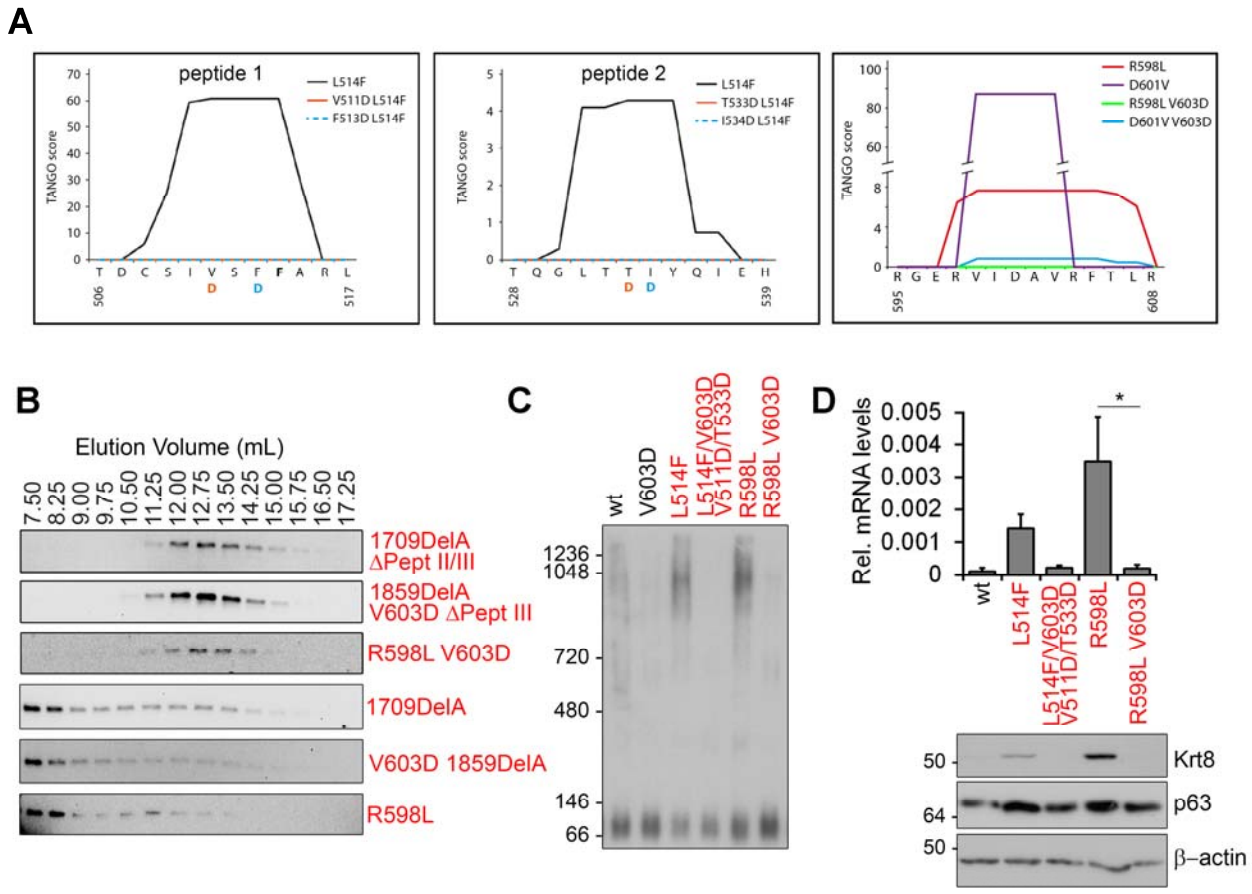

Figure S5 AEC mutant aggregation is alleviated by p63 variants predicted by TANGO

A. Graphic representation of the TANGO algorithm for the indicated p63 variants predicted to suppress aggregation of the AEC mutants. For L514F the two aggregation prone sequences in the SAM domain are shown (left and middle panel) (Table S3).

B. SEC analysis and Western blot of a selected set of rescue variants expressed in H1299 cells. All rescue mutants eluted as tetramers (fractions 11.25 to 15 ml).

C. BN-PAGE for p63 in mouse primary keratinocytes infected with retrovirus carrying wild type or mutants p63.

D. Real time RT-PCR of Krt8 (upper panel; n=4) and Western blot of Krt8 and p63 (lower panel) in mouse primary keratinocytes infected as in C. β-actin was used as loading control.

Data are shown as mean ± SEM and statistical significance was assessed using one-way ANOVA analysis. * $p \leq 0.05$.

SI TABLES

Table S1: NMR analysis of L514 mutant SAM domain. CYANA structure calculation statistics.

NOE assignment (a)	
15N-resolved NOESY-HSQC cross peaks	859
D_2O exchange NOESY cross peaks	151
Total number of NOESY cross peaks	1010
Assigned cross peaks	903 (89.4%)
Restraints	
Assigned NOE distance restraints	734 (100%)
Short range |i-j|≤1	431 (58.7%)
Medium range 1<|i-j|<5	216 (29.4%)
Long range |i-j|≥5	87 (11.9%)
Dihedral angle restraints (φ/ψ)	52
Hydrogen Bonds	46
Structure statistics (b)	
Average CYANA target function value ($Å^2$)	1.82±0.35
Average AMBER Energies (kcal/mol)	-2498±46
Restraint violations (c)	
Max. distance restraint violation (Å)	0.0
Number of violated distance restraints > 0.2 Å	0
Max. dihedral angle restraint violations (°)	6.42
Number of violated dihedral angle constraints > 5°	1
Ramachandran plot	
Residues in most favoured regions	87.2%
Residues in additionally allowed regions	11.8%
Residues in generously allowed regions	1.0%
Residues in disallowed regions	0.0%
RMSD (residues 9-69)	
Average backbone RMSD to mean (Å)	0.43±0.10
Average heavy atom RMSD to mean (Å)	0.92±0.10

(**a**) using automated NOE assignment and structure calculation functionalities of CYANA
(**b**) after restrained energy minimization with OPALp
(**c**) after energy minimization, calculated with CYANA

Table S2: β-aggregation propensity of the p63 C-terminal domain and mutants predicted by the TANGO algorithm

AEC point mutations are highlighted in bold.

	WT		L514F		G530V		D544Y	
residue number	residue	TANGO score	residue	TANGO score	residue	TANGO score	residue	TANGO score
506	T	0	T	0	T	0	T	0
507	D	0	D	0	D	0	D	0
508	C	3.893	C	5.845	C	3.857	C	3.852
509	S	16.807	S	24.985	S	16.641	S	16.621
510	I	39.745	I	59.269	I	39.275	I	39.231
511	V	40.727	V	60.736	V	40.244	V	40.199
512	S	40.727	S	60.736	S	40.244	S	40.199
513	F	40.727	F	60.736	F	40.244	F	40.199
514	L	40.448	**F**	60.547	L	39.965	L	39.921
515	A	19.002	A	28.463	A	18.781	A	18.759
516	R	0	R	0	R	0	R	0
517	L	0	L	0	L	0	L	0
518	G	0	G	0	G	0	G	0
519	C	0	C	0	C	0	C	0
520	S	0	S	0	S	0	S	0
521	S	0	S	0	S	0	S	0
522	C	0	C	0	C	0	C	0
523	L	0	L	0	L	0	L	0
524	D	0	D	0	D	0	D	0
525	Y	0	Y	0	Y	7.575	Y	0
526	F	0	F	0	F	9.646	F	0
527	T	0	T	0	T	9.908	T	0
528	T	0	T	0	T	10.485	T	0
529	Q	0	Q	0	Q	11.602	Q	0
530	G	0.296	G	0.293	**V**	42.921	G	0.293
531	L	4.136	L	4.097	L	45.118	L	4.089
532	T	4.136	T	4.097	T	44.618	T	4.089
533	T	4.321	T	4.281	T	44.496	T	4.272
534	I	4.321	I	4.281	I	44.364	I	4.272
535	Y	4.321	Y	4.281	Y	36.161	Y	4.272
536	Q	0.731	Q	0.727	Q	5.452	Q	0.725
537	I	0.731	I	0.727	I	5.104	I	0.725
538	E	0	E	0	E	0	E	0
539	H	0	H	0	H	0	H	0
540	Y	0	Y	0	Y	0	Y	0
541	S	0	S	0	S	0	S	0
542	M	0	M	0	M	0	M	0
543	D	0	D	0	D	0	D	0
544	D	0	D	0	D	0	**Y**	1.085
545	L	0	L	0	L	0	L	1.085
546	A	0	A	0	A	0	A	1.085

547	S	0	S	0	S	0	S	1.085
548	L	0	L	0	L	0	L	1.085
549	K	0	K	0	K	0	K	0
550	I	0	I	0	I	0	I	0
551	P	0	P	0	P	0	P	0
552	E	0	E	0	E	0	E	0
553	Q	0	Q	0	Q	0	Q	0
554	F	0	F	0	F	0	F	0
555	R	0	R	0	R	0	R	0
556	H	0	H	0	H	0	H	0
557	A	0	A	0	A	0	A	0
558	I	0	I	0	I	0	I	0
559	W	0	W	0	W	0	W	0
560	K	0	K	0	K	0	K	0
561	G	0	G	0	G	0	G	0
562	I	0	I	0	I	0	I	0
563	L	0	L	0	L	0	L	0
564	D	0	D	0	D	0	D	0
565	H	0	H	0	H	0	H	0
566	R	0	R	0	R	0	R	0
567	Q	0	Q	0	Q	0	Q	0
568	L	0	L	0	L	0	L	0
569	H	0	H	0	H	0	H	0
570	E	0	E	0	E	0	E	0
571	F	0	F	0	F	0	F	0
572	S	0	S	0	S	0	S	0

	WT		**1456 InsA (AEC)**		**1572 InsA (EEC)**		**1743 DelAA (EEC)**		**1709 DelA (AEC)**		**1859 DelA (AEC)**	
residue number	**residue**	**TANGO score**	**residue**	**TANGO score**	**residue**	**TANGO score**	**residue**	**TANGO score**	**residue**	**TANGO score**	**residue**	**TANGO score**
480	L	0	L	0	L	0	L	0	L	0	L	0
481	S	0	S	0	S	0	S	0	S	0	S	0
482	P	0	P	0	P	0	P	0	P	0	P	0
483	T	0	T	0	T	0	T	0	T	0	T	0
484	Q	0	Q	0	Q	0	Q	0	Q	0	Q	0
485	A	0	A	0	A	0	A	0	A	0	A	0
486	L	0	**T**	0	L	0	L	0	L	0	L	0
487	P	0	P	0	P	0	P	0	P	0	P	0
488	P	0	S	0	P	0	P	0	P	0	P	0
489	P	0	P	0	P	0	P	0	P	0	P	0
490	L	0	T	0	L	0	L	0	L	0	L	0
491	S	0	L	0	S	0	S	0	S	0	S	0
492	M	0	H	0	M	0	M	0	M	0	M	0
493	P	0	A	0	P	0	P	0	P	0	P	0
494	S	0	I	0	S	0	S	0	S	0	S	0
495	T	0	H	0	T	0	T	0	T	0	T	0
496	S	0	L	0	S	0	S	0	S	0	S	0
497	H	0	P	0	H	0	H	0	H	0	H	0

498	C	0	L	0	C	0	C	0	C	0	C	0
499	T	0	H	0	T	0	T	0	T	0	T	0
500	P	0	T	0	P	0	P	0	P	0	P	0
501	P	0	P	0	P	0	P	0	P	0	P	0
502	P	0	T	0	P	0	P	0	P	0	P	0
503	P	0	S	0	P	0	P	0	P	0	P	0
504	Y	0	V	0	Y	0	Y	0	Y	0	Y	0
505	P	0	S	0	P	0	P	0	P	0	P	0
506	T	0	H	0	T	0	T	0	T	0	T	0
507	D	0	R	0	D	0	D	0	D	0	D	0
508	C	3.893	L	0	C	3.789	C	3.797	C	3.792	C	3.812
509	S	16.807	Q	0	S	16.356	S	16.391	S	16.369	S	16.457
510	I	39.745	H	0	I	38.624	I	38.803	I	38.727	I	38.935
511	V	40.727	C	0	V	39.577	V	39.762	V	39.685	V	39.898
512	S	40.727	Q	0	S	39.577	S	39.762	S	39.685	S	39.898
513	F	40.727	F	0	F	39.577	F	39.762	F	39.685	F	39.898
514	L	40.448	L	0	L	39.305	L	39.49	L	39.413	L	39.625
515	A	19.002	S	0	A	18.464	A	18.552	A	18.515	A	18.614
516	R	0	E	0	R	0	R	0	R	0	R	0
517	L	0	V	23.371	L	0	L	0	L	0	L	0
518	G	0	G	24.559	G	0	G	0	G	0	G	0
519	C	0	L	34.323	C	0	C	0	C	0	C	0
520	S	0	F	35.7	S	0	S	0	S	0	S	0
521	S	0	I	35.801	S	0	S	0	S	0	S	0
522	C	0	M	26.495	C	0	C	0	C	0	C	0
523	L	0	S	16.056	L	0	L	0	L	0	L	0
524	D	0	G	12.223	**E**	0	D	0	D	0	D	0
525	Y	0	L	11.888	L	0	Y	0	Y	0	Y	0
526	F	0	F	9.96	F	0	F	0	F	0	F	0
527	T	0	H	0	H	0	T	0	T	0	T	0
528	T	0	D	0	D	0	T	0	T	0	T	0
529	Q	0	P	0	P	0	Q	0	Q	0	Q	0
530	G	0.296	G	0	G	0	G	0.285	G	0.284	G	0.286
531	L	4.136	A	0	A	0	L	3.982	L	3.969	L	4.003
532	T	4.136	D	0	D	0	T	3.982	T	3.969	T	4.003
533	T	4.321	H	0	H	0	T	4.16	T	4.146	T	4.182
534	I	4.321	H	0	H	0	I	4.16	I	4.146	I	4.182
535	Y	4.321	L	0	L	0	Y	4.16	Y	4.146	Y	4.182
536	Q	0.731	S	0	S	0	Q	0.703	Q	0.701	Q	0.707
537	I	0.731	D	0	D	0	I	0.703	I	0.701	I	0.707
538	E	0					E	0	E	0	E	0
539	H	0					H	0	H	0	H	0
540	Y	0					Y	0	Y	0	Y	0
541	S	0					S	0	S	0	S	0
542	M	0					M	0	M	0	M	0
543	D	0					D	0	D	0	D	0
544	D	0					D	0	D	0	D	0
545	L	0					L	0	L	0	L	0
546	A	0					A	0	A	0	A	0
547	S	0					S	0	S	0	S	0
548	L	0					L	0	L	0	L	0
549	K	0					K	0	K	0	K	0

550	I	0					I	0	I	0	I	0
551	P	0					P	0	P	0	P	0
552	E	0					E	0	E	0	E	0
553	Q	0					Q	0	Q	0	Q	0
554	F	0					F	0	F	0	F	0
555	R	0					R	0	R	0	R	0
556	H	0					H	0	H	0	H	0
557	A	0					A	0	A	0	A	0
558	I	0					I	0	I	0	I	0
559	W	0					W	0	W	0	W	0
560	K	0					K	0	K	0	K	0
561	G	0					G	0	G	0	G	0
562	I	0					I	0	I	0	I	0
563	L	0					L	0	L	0	L	0
564	D	0					D	0	D	0	D	0
565	H	0					H	0	H	0	H	0
566	R	0					R	0	R	0	R	0
567	Q	0					Q	0	Q	0	Q	0
568	L	0					L	0	L	0	L	0
569	H	0					H	0	H	0	H	0
570	E	0					E	0	**D**	0	E	0
571	F	0					F	0	S	0	F	0
572	S	0					S	0	P	0	S	0
573	S	0					S	0	P	0	S	0
574	P	0					P	0	L	0.52	P	0
575	S	0					S	0	L	0.52	S	0
576	H	0					H	0	I	0.52	H	0
577	L	0					L	0	S	0.52	L	0
578	L	0					L	0	C	0.52	L	0
579	R	0					R	0	G	0	R	0
580	T	0					T	0	P	0	T	0
581	P	0					P	0	Q	0	P	0
582	S	0					**Q**	0	A	0	S	0
583	S	0					C	0	V	0	S	0
584	A	0					L	0	P	0	A	0
585	S	0					Y	0	L	0	S	0
586	T	0					S	0	Q	0	T	0
587	V	0					Q	0	S	0	V	0
588	S	0					C	0	V	0	S	0
589	V	0					G	0	W	0	V	0
590	G	0					L	0	A	0	G	0
591	S	0					Q	0	P	0	S	0
592	S	0							V	0	S	0
593	E	0							R	0	E	0
594	T	0							P	0.088	T	0
595	R	0							G	10.371	R	0
596	G	0							V	47.019	G	0
597	E	0							S	49.615	E	0
598	R	0							V	65.539	R	0
599	V	0.867							L	65.87	V	0.837
600	I	0.867							L	65.811	I	0.837
601	D	0.867							M	58.206	D	0.837

602	A	0.867							L	49.885	A	0.837
603	V	0.867							C	11.908	V	0.837
604	R	0.867							D	0	R	0.837
605	F	0.867							S	0	F	0.837
606	T	0.497							P	0	T	0.479
607	L	0.497							S	0	L	0.479
608	R	0							A	0	R	0
609	Q	0							R	0	Q	0
610	T	0							P	0	T	0
611	I	0							S	0	I	0
612	S	0							L	0	S	0
613	F	0							S	0	F	0
614	P	0							H	0	P	0
615	P	0							P	0	P	0
616	R	0							E	0	R	0
617	D	0							M	0	D	0
618	E	0							S	0	E	0
619	W	0							G	0	W	0.442
620	N	0							M	0.553	**M**	0.694
621	D	0							T	1.091	T	1.234
622	F	0							S	2.448	S	2.598
623	N	0							T	13.776	T	13.969
624	F	0							L	32.82	L	33.083
625	D	0							T	36.223	T	36.499
626	M	0							W	41.541	W	41.837
627	D	0							M	42.797	M	43.097
628	A	0							L	42.722	L	43.021
629	R	0							A	39.749	A	40.037
630	R	0							A	36.95	A	37.228
631	N	0							I	34.167	I	34.435
632	K	0							S	3.695	S	3.709
633	Q	0							N	0	N	0
634	Q	0							S	0	S	0
635	R	0							A	0	A	0
636	I	0							S	0	S	0
637	K	0							K	0	K	0
638	E	0							R	0	R	0
639	E	0							R	0	R	0
640	G	0							G	0	G	0
641	E	0							S	0	S	0
642									E	0	E	0
643									P	0	P	0
644									H	0	H	0
645									H	0	H	0
646									V	0	V	0
647									S	0	S	0
648									S	0	S	0
649									S	0	S	0
650									Y	0	Y	0
651									P	0	P	0
652									S	0	S	0
653									P	0	P	0

654									N	0	N	0
655									C	0	C	0
656									Q	0	Q	0
657									P	0	P	0
658									P	0	P	0
659									K	0	K	0
660									S	0	S	0
661									T	0	T	0
662									P	0	P	0
663									A	0	A	0

	WT		V603D		R598L		D601V		R598L V603D		D601V V603D	
residue number	residue	TANGO score	residue	TANGO score	residue	TANGO score	residue	TANGO score	residue	TANGO score	residue	TANGO score
594	T	0	T	0	T	0	T	0	T	0	T	0
595	R	0	R	0	R	0	R	0	R	0	R	0
596	G	0	G	0	G	0	G	0	G	0	G	0
597	E	0	E	0	E	0	E	0	E	0	E	0
598	R	0	R	0	**L**	6.443	R	0	**L**	0	R	0
599	V	0.854	V	0	V	7.648	V	87.234	V	0	V	0.825
600	I	0.854	I	0	I	7.648	I	87.234	I	0	I	0.825
601	D	0.854	D	0	D	7.648	**V**	87.234	D	0	**V**	0.825
602	A	0.854	A	0	A	7.648	A	87.234	A	0	A	0.825
603	V	0.854	<u>D</u>	0	V	7.648	V	87.234	<u>D</u>	0	<u>D</u>	0.825
604	R	0.854	R	0	R	7.648	R	0	R	0	R	0.825
605	F	0.854	F	0	F	7.648	F	0	F	0	F	0.825
606	T	0.489	T	0	T	7.293	T	0	T	0	T	0.474
607	L	0.489	L	0	L	6.091	L	0	L	0	L	0.474
608	R	0	R	0	R	0	R	0	R	0	R	0
609	Q	0	Q	0	Q	0	Q	0	Q	0	Q	0
610	T	0	T	0	T	0	T	0	T	0	T	0
611	I	0	I	0	I	0	I	0	I	0	I	0
612	S	0	S	0	S	0	S	0	S	0	S	0
613	F	0	F	0	F	0	F	0	F	0	F	0
614	P	0	P	0	P	0	P	0	P	0	P	0
615	P	0	P	0	P	0	P	0	P	0	P	0
616	R	0	R	0	R	0	R	0	R	0	R	0

Table S3: β-aggregation propensity of the p63L514F and its rescue variants predicted by the TANGO algorithm

The L514F point mutation is highlighted in bold, while the suppression mutations are underlined.

	WT	L514F	L514F V511D	L514F F513D	L514F T533D	L514F I534D

residue number	residue	TANGO score	residue	TANGO score	residue	TANGO score	residue	TANGO score	residue	TANGO score	residue	TANGO score
506	T	0	T	0	T	0	T	0	T	0	T	0
507	D	0	D	0	D	0	D	0	D	0	D	0
508	C	3.893	C	5.845	C	0	C	0	C	5.859	C	5.859
509	S	16.807	S	24.985	S	0	S	0	S	25.046	S	25.046
510	I	39.745	I	59.269	I	0	I	0	I	59.369	I	59.369
511	V	40.727	V	60.736	D	0	V	0	V	60.837	V	60.837
512	S	40.727	S	60.736	S	0	S	0	S	60.837	S	60.837
513	F	40.727	F	60.736	F	0	D	0	F	60.837	F	60.837
514	L	40.448	**F**	60.547	**F**	0	**F**	0	**F**	60.649	**F**	60.649
515	A	19.002	A	28.463	A	0	A	0	A	28.511	A	28.511
516	R	0	R	0	R	0	R	0	R	0	R	0
517	L	0	L	0	L	0	L	0	L	0	L	0
518	G	0	G	0	G	0	G	0	G	0	G	0
519	C	0	C	0	C	0	C	0	C	0	C	0
520	S	0	S	0	S	0	S	0	S	0	S	0
521	S	0	S	0	S	0	S	0	S	0	S	0
522	C	0	C	0	C	0	C	0	C	0	C	0
523	L	0	L	0	L	0	L	0	L	0	L	0
524	D	0	D	0	D	0	D	0	D	0	D	0
525	Y	0	Y	0	Y	0	Y	0	Y	0	Y	0
526	F	0	F	0	F	0	F	0	F	0	F	0
527	T	0	T	0	T	0	T	0	T	0	T	0
528	T	0	T	0	T	0	T	0	T	0	T	0
529	Q	0	Q	0	Q	0	Q	0	Q	0	Q	0
530	G	0.296	G	0.293	G	0.294	G	0.294	G	0	G	0
531	L	4.136	L	4.097	L	4.111	L	4.111	L	0	L	0
532	T	4.136	T	4.097	T	4.111	T	4.111	T	0	T	0
533	T	4.321	T	4.281	T	4.295	T	4.295	D	0	T	0
534	I	4.321	I	4.281	I	4.295	I	4.295	I	0	D	0
535	Y	4.321	Y	4.281	Y	4.295	Y	4.295	Y	0	Y	0
536	Q	0.731	Q	0.727	Q	0.729	Q	0.729	Q	0	Q	0
537	I	0.731	I	0.727	I	0.729	I	0.729	I	0	I	0
538	E	0	E	0	E	0	E	0	E	0	E	0
539	H	0	H	0	H	0	H	0	H	0	H	0
540	Y	0	Y	0	Y	0	Y	0	Y	0	Y	0
541	S	0	S	0	S	0	S	0	S	0	S	0
542	M	0	M	0	M	0	M	0	M	0	M	0
543	D	0	D	0	D	0	D	0	D	0	D	0
544	D	0	D	0	D	0	D	0	D	0	D	0
545	L	0	L	0	L	0	L	0	L	0	L	0
546	A	0	A	0	A	0	A	0	A	0	A	0
547	S	0	S	0	S	0	S	0	S	0	S	0
548	L	0	L	0	L	0	L	0	L	0	L	0
549	K	0	K	0	K	0	K	0	K	0	K	0
550	I	0	I	0	I	0	I	0	I	0	I	0
551	P	0	P	0	P	0	P	0	P	0	P	0
552	E	0	E	0	E	0	E	0	E	0	E	0
553	Q	0	Q	0	Q	0	Q	0	Q	0	Q	0

554	F	0	F	0	F	0	F	0	F	0	F	0
555	R	0	R	0	R	0	R	0	R	0	R	0
556	H	0	H	0	H	0	H	0	H	0	H	0
557	A	0	A	0	A	0	A	0	A	0	A	0
558	I	0	I	0	I	0	I	0	I	0	I	0
559	W	0	W	0	W	0	W	0	W	0	W	0
560	K	0	K	0	K	0	K	0	K	0	K	0
561	G	0	G	0	G	0	G	0	G	0	G	0
562	I	0	I	0	I	0	I	0	I	0	I	0
563	L	0	L	0	L	0	L	0	L	0	L	0
564	D	0	D	0	D	0	D	0	D	0	D	0
565	H	0	H	0	H	0	H	0	H	0	H	0
566	R	0	R	0	R	0	R	0	R	0	R	0
567	Q	0	Q	0	Q	0	Q	0	Q	0	Q	0
568	L	0	L	0	L	0	L	0	L	0	L	0
569	H	0	H	0	H	0	H	0	H	0	H	0
570	E	0	E	0	E	0	E	0	E	0	E	0
571	F	0	F	0	F	0	F	0	F	0	F	0
572	S	0	S	0	S	0	S	0	S	0	S	0

Table S4: List of oligonucleotide primers used in this study

Oligonucleotide primers for mutagenesis and cloning.		
Mutation	**Forward 5'-3'**	**Reverse 5'-3'**
E639X	CAGCGCATCAAAGAGTAGGGGGAGTGAGCC	GGCTCACTCCCCCTACTCTTTGATGCGCTG
Q634X	CGCCGCAATAAGCAATAGCGCATCAAAGAGGAG	CTCCTCTTTGATGCGCTATTGCTTATTGCGGCG
1709DelA94	CCGGCAGCTCCACGATTCTCCTCCCCTTCT	AGAAGGGGAGGAGAATCGTGGAGCTGCCGG
1859DelA	CCCCGAGATGAGTGGATGACTTCAACTTTGACATGG	CCATGTCAAAGTTGAAGTCATCCACTCATCTCGGGG
1709DelA (cloning)	CCCGGCGGCCGCGTTGTACCTGGAAAACAATGCCC	AGATCATCCATGGAGTAATGCTC
1859DelA (cloning)	GAGCATTACTCCATGGATGATCT	GCGGAGATCTTCCCCTAAGAAATCAGACAAGAGG
pBABE-DNp63a (cloning)	CCCGGGATCCCTCGTTTAGTGAACCGTCAGAATTG	CCGGATCCTCATTCTCCTTCCTCTTTGATACGCTG
p63L514F V511D	CGTATCCCACAGATTGCAGCATTGATAGTTTCTTTGCGAGGTTGGGCTGTTC	GAACAGCCCAACCTCGCAAAGAAACTATCAATGCTGCAATCTGTGGGATACG
p63L514F F513D	CCACAGATTGCAGCATTGTCAGTGATTTTGCGAGGTTGGGCTGTTC	GAACAGCCCAACCTCGCAAAATCACTGACAATGCTGCAATCTGTGG
p63T533D	CGACCCAGGGGCTGACCGATATCTATCAGATTGAGCATTACTCC	GGAGTAATGCTCAATCTGATAGATATCGGTCAGCCCCTGGGTCG

p63I534D	CCAGGGGCTGACCACCGATTATCAGATTGAGCATTACTCCATG	CATGGAGTAATGCTCAATCTGATAATCGGTGGTCAGCCCCTGG
p631709DelA ΔPept II	CTCCAGTGAGACCCGGGGATTCACCCTCCGCCAGAC	GTCTGGCGGAGGGTGAATCCCCGGGTCTCACTGGAG
p631709DelA ΔPept III	GAGATGAGTGGAATGACTTCAACTAGCAACAGCGCATCAAAGAGG	CCTCTTTGATGCGCTGTTGCTAGTTGAAGTCATTCCACTCATCTC
p631859DelA ΔPept III	GAGATGAGTGGATGACTTCAACTAGCAACAGCGCATCAAAGAGG	CCTCTTTGATGCGCTGTTGCTAGTTGAAGTCATCCACTCATCTC
p633'ss-int10/1456InsA ΔPept I	CAGCATTGTCAGTTTCTTAGCGAGCACGACCCAGGGGCTG	CAGCCCCTGGGTCGTGCTCGCTAAGAAACTGACAATGCTG
p63R598L V603D	GTGAGACCCGGGGTGAGCTGGTTATTGATGCTGACCGATTCACC	GGTGAATCGGTCAGCATCAATAACCAGCTCACCCCGGGTCTCAC
p63D601V V603D	CCCGGGGTGAGCGTGTTATTGTGGCTGACCGATTCACCCTCCGCCAG	CTGGCGGAGGGTGAATCGGTCAGCCACAATAACACGCTCACCCCGGG
Oligonucleotide primers for Real Time RT-PCR		
Gene	**Forward 5'-3'**	**Reverse 5'-3'**
mTrp63 ex12-13 wt	ACTCTCCATGCCCTCCAC	GAGCAGCCCAACCTTGCT
mTrp63 ex12-13 L514F	ACTCTCCATGCCCTCCAC	GAGCAGCCCAACCTTGCA
mActb	CTAAGGCCAACCGTGAAAAGAT	GCCTGGATGGCTACGTACATG
mKrt5	CAACGTCAAGAAGCAGTGTGC	TTGCTCAGCTTCAGCAATGG
mKrt14	GATGTGACCTCCACCAACCG	CCATCGTGCACATCCATGAC
mDsc3	CCACCGTCTCTCACTACATGGA	TGTCCTGAACTTTCATTATCAGTTTGT
mIrf6	CAGCTCTCTCCCCATGACTGA	CCCATACTCCTTCCCACGATAC
mFgfr2	TGGATCGAATTCTGACTCTCACA	TTCGAGAGGCTGGGTGAGAT
mSmad7	AACGAGAGTCAGCACTGCCA	GAAGGTGGTGCCCACTTTCA
mCdkn1a	GAACATCTCAGGGCCGAAAA	CAATCTGCGCTTGGAGTGAT
mKrt8	TGCTCATGTTCTGCATCCCA	GATCACCACCTACCGCAAGC
hKRT14	GGATGACTTCCGCACCAAGT	TCCACACTCATGCGCAGGT
hIRF6	CAGCTCTCTCCCCATGACTGA	CCCATACTCCTTCCCACGATAC
hDSC3	CCACCGTCTCTCACTACATGGA	TGTCCTGAACTTTCATTATCAGTTTGT
Oligonucleotide primers for ChIP-qPCR.		
p63 binding site	**Forward 5'-3'**	**Reverse 5'-3'**

human P63 enhancer	CGTTCCAAAGCCTAACCTGATCA	TTTTCCCAAACTCCAACCTG
human FGFR2 enhancer	CCCCGTGGCCGAAAA	GAAAGCGCAGGCGAGTTCT
human KRT14 promoter	GGGCCTGTCTGAGGAGATAGG	AGGCATGTTGAGAGGAATGTGA
human CDKN1A promoter	TTCAAGGCAGTGGGAGAAGG	TGGTTGTCAAATGTCCAGCAG
mouse p63 enhancer	CTGCGTGTGCGTTGCATATAA	CGTCATGTCTCCCTGCCTTC
mouse Irf6 enhancer	AGCCTCCCAGTTACAAGTAGCAA	TGCCACCACTTTCCCAGTCT
mouse Fgfr2 enhancer	GGGCGCCTGATTGCTTT	CAGCCTGGACTCATTTTCATCTG
mouse Smad7 promoter	GTGAGGCGAAAGAAGAGCCC	GCTCTGACTGGCTTGTATGCC
mouse Krt8 enhancer	GCCATACCCAGGCATCCATA	CACACAACACCCACTACCCCT
Oligonucleotide primers for the generation of the conditional knock-in construct.		
Ap63CDNU	ATTAGCGGCCGCGTAGAGGAGCCAAAATTTGCTGAC	
Ap63CDNL	GCCGAAGCTTGCACTGCCTTCTATCCCCACAC	
Bp63CDNU	GCCGAAGCTTCAATCATAAGAGCTCTTAACATCAC	
Bp63CDNL	GCCGACTAGTTGAGCACAGATTCCTCTGTGGGAC	
CmP63U	ATTAGCGGCCGCCAGAGGCACATGTAGCCCCACAG	
CmP63L	GCCGGAATTCTTGGGGGGTCTCTTAGGATGTTTCA	
DmP63U	ATTAGGATCCGCACAAAATAGCCAATATAGT	
DmP63L	ATTAGTCGACGCTGAGGTCCAAGGAGTGCTCC	
C1P63U	ATTAGCGGCCGCATGCAGGAAACTCAATCCCCA	
C1P63L	GCCGGAATTCAGTTAAATGAGAAGGCAAAAGTCTC	
D1P63U	ATTAGGATCCGCGCCCATTGCGGGGTTCTTCC	
D1P63L	GCCGGTCGACTTAGACTATAAGGCTGAAAATGC	
P63ex14fgU	GTTACAAACTTCAAGGCCTGTTAGC	
P63ex14fgL	TAATCCCGGGCTTCTCCTTCCTCTTTGATACGCTG	
ISceIE14U	GCCGAGTTACGCTAGGGATAACAGGGTAATATAGGCCGTCTGCACTATTTTACACA	
ICeuIFlagL	GCCGTTCGCTACCTTAGGACCGTTATAGTTACGGGATCACTACTTGTCATCGTC	
DmP63U2	ATTAGCGGCCGCGCACAAAATAGCCAATATAGT	
Ex13L2	GCTCAATCTGATAGATGGTGGTC	

Ex13U2	GACCACCATCTATCAGATTGAGC	
RecEx14L3	ATTAGAATTCAGATCTCATTCTCCTTCCTCTTTGATACGC	
DmP63U	ATTAGGATCCGCACAAAATAGCCAATATAGT	
Ex13MutL	CCCAACCTTGCAAAGAAACTGC	
Ex13mutU	GCAGTTTCTTTGCAAGGTTGGG	
RecEx13L	ATTAGTCGACTTTTTAACCAATCTCTGAGTAAG	
Oligonucleotide primers for Screening PCR of ES cells.		
name	**Forward 5'-3'**	**Reverse 5'-3'**
5'Arm	TATAGTCCCAGTGCTGCAAGTGCT	GATCCCATGGTTTAGTTCCTCACC
3'Arm	ATGGCTTCTGAGGCGGAAAGAACCAG	AAGCCCCATGAAATGACACGACAGAAT
Oligonucleotide primers for mouse genotyping.		
L514F3xFlag For	CAGCGTATCAAAGAGGAAGGAGA	
L514F3xFlag Rev	AGCCAGAATCAGAATCAGGTGAC	

Table S5: List of antibodies used in this study

Antibodies		
rabbit polyclonal anti-p63 (H137)	Santa Cruz Biotechnology	Cat#sc-8343
mouse monoclonal anti-p63 (4A4)	Santa Cruz Biotechnology	Cat#sc-8431
rabbit anti-Keratin 14	Covance	Cat#PRB-155P
mouse monoclonal anti-ß-Actin (AC-15)	Santa Cruz Biotechnology	Cat#sc-69879
rabbit anti-IRF6	Ferone et al., 2012 (1)	N/A
mouse monoclonal anti-p73	Millipore	Cat# OP109L
goat polyclonal anti-HA	Bethyl Laboratories	Cat# A190-138A
rabbit polyclonal anti-ERK1 (K-23)	Santa Cruz Biotechnology	Cat# sc-94
mouse monoclonal anti-Myc (4A6)	Millipore	Cat# 05-724
normal mouse IgG	Santa Cruz Biotechnology	Cat# sc-2025
normal rabbit IgG	Santa Cruz Biotechnology	Cat# sc-2027
sheep anti-mouse IgG HRP	GE Healthcare	Cat# NA931
donkey anti-rabbit IgG HRP	GE Healthcare	Cat# NA934

References

1. Ferone G*, et al.* (2012) Mutant p63 causes defective expansion of ectodermal progenitor cells and impaired FGF signalling in AEC syndrome. *EMBO molecular medicine* 4(3):192-205.
2. Candi E*, et al.* (2006) Differential roles of p63 isoforms in epidermal development: selective genetic complementation in p63 null mice. *Cell death and differentiation* 13(6):1037-1047.
3. Kern SE*, et al.* (1992) Oncogenic forms of p53 inhibit p53-regulated gene expression. *Science* 256(5058):827-830.
4. Antonini D*, et al.* (2015) A composite enhancer regulates p63 gene expression in epidermal morphogenesis and in keratinocyte differentiation by multiple mechanisms. *Nucleic acids research* 43(2):862-874.
5. Takahashi K & Yamanaka S (2006) Induction of pluripotent stem cells from mouse embryonic and adult fibroblast cultures by defined factors. *Cell* 126(4):663-676.
6. Chen Y, Mistry DS, & Sen GL (2014) Highly rapid and efficient conversion of human fibroblasts to keratinocyte-like cells. *The Journal of investigative dermatology* 134(2):335-344.
7. Liu P, Jenkins NA, & Copeland NG (2003) A highly efficient recombineering-based method for generating conditional knockout mutations. *Genome research* 13(3):476-484.
8. Gebel J*, et al.* (2016) Mechanism of TAp73 inhibition by DeltaNp63 and structural basis of p63/p73 hetero-tetramerization. *Cell death and differentiation* 23(12):1930-1940.
9. Guntert P & Buchner L (2015) Combined automated NOE assignment and structure calculation with CYANA. *Journal of biomolecular NMR* 62(4):453-471.
10. Guntert P, Mumenthaler C, & Wuthrich K (1997) Torsion angle dynamics for NMR structure calculation with the new program DYANA. *Journal of molecular biology* 273(1):283-298.
11. Shen Y, Delaglio F, Cornilescu G, & Bax A (2009) TALOS+: a hybrid method for predicting protein backbone torsion angles from NMR chemical shifts. *Journal of biomolecular NMR* 44(4):213-223.
12. Koradi R, Billeter M, & Guntert P (2000) Point-centered domain decomposition for parallel molecular dynamics simulation. *Comput Phys Commun* 124(2-3):139-147.
13. Ponder JW & Case DA (2003) Force fields for protein simulations. *Advances in protein chemistry* 66:27-85.
14. Romano RA, Birkaya B, & Sinha S (2007) A functional enhancer of keratin14 is a direct transcriptional target of deltaNp63. *The Journal of investigative dermatology* 127(5):1175-1186.
15. Benjwal S, Verma S, Rohm KH, & Gursky O (2006) Monitoring protein aggregation during thermal unfolding in circular dichroism experiments. *Protein science : a publication of the Protein Society* 15(3):635-639.
16. Martinez Molina D*, et al.* (2013) Monitoring drug target engagement in cells and tissues using the cellular thermal shift assay. *Science* 341(6141):84-87.